Analysis of an Underwater Periodic Helmholtz-Type Noise Mitigation System for Offshore Impact Pile Driving

G. M. de Wit

Delft University of Technology

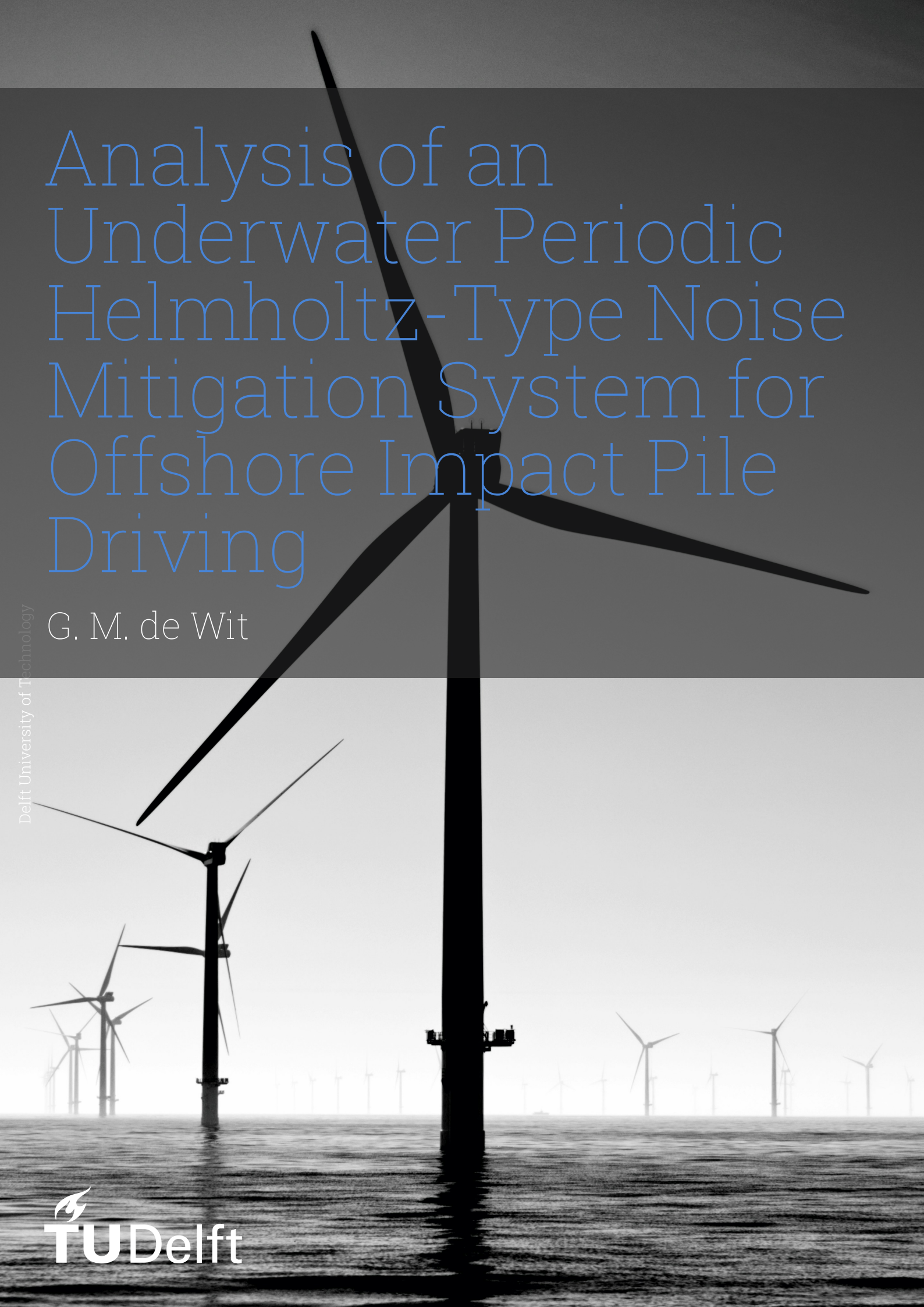

TU Delft

Analysis of an Underwater Periodic Helmholtz-Type Noise Mitigation System for Offshore Impact Pile Driving

by

G. M. de Wit

to obtain the degree of Master of Science

at the Delft University of Technology,

to be defended publicly on Wednesday August 28, 2024 at 10:00 AM.

Student number:	4596897	
Project duration:	December 18, 2023 – August 28, 2024	
Thesis committee:	Dr. ir. A. Tsouvalas,	TU Delft, chair
	Dr. ir. A. B. Faragau,	TU Delft, supervisor
	Ir. Y. Peng,	TU Delft, supervisor
	Ing. B. Jongenburger,	Seaway7, supervisor
	Ir. L. van Hagen,	Seaway7, supervisor

Cover photo by Nicholas Doherty on Unsplash

An electronic version of this thesis is available at http://repository.tudelft.nl/.

TU Delft seaway 7

Preface

"Hence any one, even if he has no ear for music or is quite unpractised in detecting musical sounds, is put in a condition to pick the required simple tone, even if comparatively faint, from out of a great number of others. The proper tone of the resonator may even be sometimes heard cropping up in the whistling of the wind, the rattling of carriage wheels, the splashing of water." [19]

I came across this passage while reading through a section of *On the Sensations of Tone as a Physiological Basis for the Theory of Music* by Hermann von Helmholtz, first translated to the English language in 1875. It describes the composition of noise in a very simple and understandable manner; as a superposition of a great number of tones (or frequencies), and it described the possibility to distinguish between the individual tones through a resonating device. It amazes me that this technology, initially purposed for music, is now applied in complex industries such as the automotive, maritime and energy sector.

During the first few weeks of this research I gradually became acquainted to the abstract field of underwater acoustics. Thank you, Yaxi, for guiding me through this period and for your help in building a basis of fundamental knowledge of this field. After some time, the level of abstractness of this research increased when the field of acoustic metamaterials became relevant. Andrei, thank you for introducing me to this remarkable field and for always making time for discussions, and for making me think twice about my own questions. Additionally, I want to thank Apostolos Tsouvalas for always showing great interest in my research and constructively criticising my work, which ever motivated me.

Finally, I would like to show my gratitude to Seaway7 for providing me with the means to conduct this research and for giving me the time and space to grow during this research. Bas and Luuk, thank you for your patience during our weekly meetings discussing the seemingly never ending supply of plots, and for keeping me sharp whilst I was inside the bubble of my own research. Thank you, Jeroen, and the rest of the Development Team, for making me feel at home at Seaway7 and for providing me with a very motivating work environment.

And to the reader of this thesis; I hope that it sparks your interest in underwater noise mitigation and its importance in reducing a small part of the burden that we put upon our natural environment as a modern society.

Abstract

Several studies have highlighted the negative impact of underwater impact pile driving on marine life, underscoring the need for effective noise mitigation systems (NMS). While bubble curtains are commonly used, recent research also focuses on near-pile NMSs. For instance, with resonating devices such as Helmholtz resonators, which are known for their tunability and effectiveness in specific frequency ranges. However, the potential for broadband noise mitigation using arrays of Helmholtz resonators in offshore impact pile driving remains uncertain. This thesis aims to address this research gap.

Locally resonant acoustic metamaterials, characterised by unusual properties such as negative or zero-valued effective mass, have shown potential for broadband noise mitigation. This thesis defines an acoustic metamaterial composed of Helmholtz-type resonators and investigates its combined effects. The study employs the finite element method (FEM) and the lumped-component method to define the resonator characteristics of a reference Helmholtz-type resonator. Subsequently, the boundary element method (BEM) is used to examine the acoustic behaviour of horizontal arrays of Helmholtz-type resonators, appropriately named Helmholtz-type acoustic metamaterials, in the frequency domain. Multiple configurations of these systems are analysed. Finally, a case study approximating the pressure field radiated by a vibrating monopile excited by an impact hammer is conducted in the time domain using the FEM.

The results indicate that Helmholtz-type acoustic metamaterials amplify sound pressure at frequencies below the natural frequency of the individual resonators and reduce it at frequencies above. Functional grading, achieved by incrementally decreasing the natural frequencies of the individual resonators in steps of up to 3 Hz along each horizontal array, can reduce the low-frequency amplification while maintaining the high-frequency attenuation. In a vertical system of Helmholtz-type acoustic metamaterials similar behaviour is observed. A vertical system comprising of horizontal arrays of 20 resonators with a horizontal spacing of 0.1 meter and a vertical spacing of 1 meter between each array shows a promising balance between attenuation and unwanted amplification. However, the system's performance is sensitive to maintaining optimal volume of encapsulated air within the resonators, as the target frequency can significantly increase if a large percentage of the encapsulated air is lost. The transient response behaviour aligns with frequency domain observations, showing low-frequency amplification and high-frequency mitigation. Additionally, it is found that the orientation of the resonators does not significantly affect the transient response. Finally, it is important to note that mechanical coupling effects, which are not included in this study, may introduce additional low-frequency interactions.

This study demonstrates the potential of using Helmholtz-type acoustic metamaterials in near-pile NMSs for offshore impact pile driving, emphasising the system's sensitivity to the frequency of the applied force and the importance of air volume maintenance. The findings suggest that while Helmholtz-type resonators can effectively mitigate noise in specific frequency ranges, careful configuration is crucial for achieving broadband noise mitigation and for minimising the risk of unwanted amplification of the pressure field.

Contents

1

Introduction

Recently, the Dutch government published plans to install a total of 21 GW of offshore wind capacity in the North Sea before the end of 2032 [34]. The largest wind farm that is currently operational has a total capacity of 1529 MW, comprising of 139 11 MW wind turbines on monopile foundations with a diameter of 7-8 meter and a length of 76.5 meter [35][14]. In the near-future, it is expected that the size of the monopiles will increase to at least a diameter of 11 meters and a length of 105 meters to support the increasing size of offshore wind turbines [15].

Studies have shown that the underwater noise radiated during the installation of offshore foundation piles can cause behavioural disturbances for ocean life [3][12]. For instance, bottlenose dolphins have a threshold for behavioural disturbances at noise levels of 140 dB re 1 μPa (peak-to-peak broadband level) at distances of up to 50 km from the source [45]. Additionally, oceanic fish species such as cod and sole show behavioural anomalies starting at peak pressure levels ($L_{p,peak}$) of 140 dB re 1 μPa [31]. Similarly, pile-driving noise disrupts the structure and dynamics of sea bass shoals, where reduced cohesiveness, directional ordering and speed correlation are observed [20]. To reduce the impact of underwater noise on marine life, the German Federal Environmental Agency set limitations for offshore noise in 2011 [5]. The limitations for the Sound Exposure Level (L_E) and $L_{p,peak}$ are 160 dB re 1 μPa and 190 dB re 1 μPa, respectively, measured at 750 meters from the source. To comply with the imposed limitations, offshore contractors apply Noise Mitigation Systems (NMS).

At the FINO III test site in the German Bight, measurements of the pile-driving noise during the monopile installation for the DanTysk offshore wind farm have been conducted [16]. The FINO III hydrophone, located 3.8 kilometres from the studied monopile, measured consistently L_p levels of around 165 dB re 1 μPa. During construction, Big Bubble Curtains (BBCs) were used as a pile-driving NMS. The NMS achieved a noise reduction ranging from 7 to 12 dB re 1 μPa (L_p). This led to a significant decrease in the oceanic area impacted by pile driving noise, with up to a 75% reduction compared to scenarios where pile driving was conducted without any noise mitigation measures [10]. This is in agreement with measurements at the Borkum West II offshore wind farm, where a reduction of the exposed ocean area of 90% has been recorded [33]. At both projects, the BBCs show the highest attenuation at frequencies above 1000 Hz. For animals such as harbour porpoises and bottlenose dolphins, the threshold for behavioural anomalies is lower at high frequencies [12][10]. Therefore, the BBCs show a positive effect on the affected marine mammals.

As mentioned in the previous paragraph, the BBCs show the highest attenuation at frequencies above 1000 Hz. However, results from the measurements conducted at DanTysk and Borkum West II show that the most energy propagates at frequencies below 1000 Hz [16][33]. In order to be in agreement with the imposed broadband noise restrictions, systems that target specific low-frequency ranges and systems that target broadband frequency ranges are being developed. An example of a broadband NMS is the IHC Noise Mitigtion Screen (IHC-NMS). According to

the German Federal Maritime and Hydrographic Agency (FMHA), the IHC-NMS can facilitate a broadband noise attenuation of 17 dB (SEL)[29]. A downside to the IHC-NMS is its size and weight, making its logistics an obstruction for efficient use. An example of a lightweight NMS is the Hydro Sound Damper, for which the FMHA reports a maximum broadband attenuation of 12 dB (SEL) with the side note that the noise attenuation is mainly in the low-frequency range [30]. The HSD can be used in combination with a BBC to realise broadband attenuation. Another low-frequency NMS is a near-pile window blind-like system based on Helmholtz resonance, currently under development by AdBm Technologies [1]. Panels of inverted open-ended cups, naturally filled with air during deployment and with specific natural frequencies provide noise attenuation in a specific frequency range, similar to the working principle of a traditional Helmholtz resonator. Because of its simplicity and high tune-ability, the Helmholtz resonator shows potential to be successfully applied noise reduction campaigns for offshore impact pile driving. However, research on the behaviour of such an NMS has not yet been widely published.

Nonetheless, the field of underwater noise propagation has been widely studied. For instance, Jensen et al. (2011) published a comprehensive book on computational ocean acoustics [23], and Reinhall and Dahl (2011) first developed a numerical method describing the noise from offshore impact pile driving [40]. In 2014, several research groups contributed to the first benchmark case for the modelling of sound emissions from offshore impact pile driving, called COMPILE [26]. Subsequently, the modelling of NMSs gained momentum. Tsouvalas (2015, 2016) introduced a semi-analytical model capable of including an air-bubble curtain in a waveguide [51][49][52]. More recently, Peng at al (2018) published results of a semi-analytical study on the behaviour of a Helmholtz resonator based NMS [37]. In order to thoroughly understand the behaviour of NMSs for offshore impact piling, studies like the aforementioned in combination with field testing is critical. Any near-field noise mitigation system should be thoroughly checked for performance at the low end of the frequency spectrum as data has shown that emitted sound can be amplified at low frequencies when such systems are deployed.

1.1. Knowledge Gap and Novelty

In 2014, Wochner et al. published a paper on the attenuation of low frequency underwater noise using arrays of air-filled resonators [56]. They reported the results of laboratory measurements and lake tests of the noise attenuation of a prototype open-ended resonator design, based on the principle of Helmholtz resonance. Moreover, Wochner published a new paper in 2016, where they conducted field tests at a monopile installation site in the North Sea [55]. However, these tests where conducted in the far field, while the system is supposed to be deployed in the near field. Peng et al. (2018) researched the behaviour of a vertical array (a single layer) of underwater Helmholtz-type resonators using the Boundary Element Method (BEM) and Finite Element Method (FEM) [37]. The key finding in their work is that the NMS is sensitive to unwanted amplifications, and that this can be mitigated by using resonators with different properties. *By doing this, a wider band of noise reduction can be achieved and the [constructive] interference can be mitigated*, Peng et al. (2018).

To the authors knowledge, the interaction of acoustically coupled Helmholtz resonators in periodic (i.e. evenly spaced) horizontal arrays has not yet been researched in the field of noise mitigation for offshore impact pile driving. However, the study of periodic structures has a long history in the field of acoustics. For instance, methods previously devised to address damping and nonlinear effects in structural dynamics offer valuable insights for tackling the challenge of wave propagation in periodic materials and structures [22]. To fully understand the behaviour of a periodic NMS, it is important to investigate the acoustic coupling between individual resonators in an array and its subsequent influence on a two-dimensional, depth dependent NMS. Furthermore, (numerical) modelling of Helmholtz-type resonators in this application has not been widely conducted. Therefore, this thesis aims to contribute to the knowledge base of periodic, low-frequency NMSs for offshore impact pile driving through literature research, semi-analytical modelling and numerical modelling.

1.2. Research Questions and Thesis Layout

On the basis of the knowledge gap and novelty introduced in the previous paragraph, a research question and two research sub-questions are drafted. The main research question reads

What is the optimal configuration of a periodic Helmholtz-type NMS for offshore impact pile driving?

The configuration of the periodic Helmholtz-type NMS is tested on the sensitivity of its lattice constant (e.g. the horizontal distance between each resonator) and the vertical distance between each horizontal section on the noise attenuation of the NMS and the characteristics of the individual resonators. Additionally, different combinations of resonators, based on their characteristics, are researched. Two modelling tools are used to answer the research question: the FEM is used to determine the pressure at the open end of a resonator, which is then used to define the resonator characteristics. Additionally, the BEM is used to model the periodic Helmholtz-type NMS.

On resonator level, two research sub-questions are included. Firstly, the effect of air escaping from the resonators is investigated by testing the sensitivity of the amount (in mass) of air inside the Helmholtz-type resonators on the noise attenuation of the NMS. Secondly, the sensitivity of the tilt of the resonators inside the NMS and its impact on the noise attenuation of the NMS is tested.

A *How does the air-water ratio of the resonators inside a Helmholtz-type NMS influence its noise reduction properties?*

B *How does the tilt of the resonators inside a Helmholtz-type NMS influence its noise reduction properties?*

In the next chapter, historical background and relevant literature on Helmholtz resonators and acoustic metamaterials is discussed. Chapter 3 discussed the solution method for solving the wave equation for pressure, and subsequently the setup of the BEM and FEM models that are used in this thesis. The depth-dependent Helmholtz resonator characteristics are defined in chapter 4, which is required to answer the first research sub-question. In chapter 5, the influence of the horizontal spacing between the individual resonators on the noise attenuation of a Helmholtz resonator based NMS is discussed. Furthermore, the influence of different air volumes inside the resonators on the noise attenuation of a Helmholtz resonator based NMS is discussed in chapter 6. The influence of the tilt of the resonators inside the Helmholtz resonator based NMS is studied in chapter 7. From this, the second research sub-question can be answered. Finally, the conclusions are given in chapter 8. Additionally, the limitations of this thesis and the authors recommendations for research improvements are provided.

1.3. Scope

In this section, the key assumptions considered in this thesis are briefly discussed.

1. The dynamics of a monopile excited by an impact hammer are not examined and the pile-driving process is not modelled. The vibrating monopile is represented by a point source (chapter 4, chapter 5, chapter 6), or by an array of phased point sources (chapter 7).
2. This thesis does not examine the propagation of acoustic pressure waves through soil. The soil is represented by a rigid boundary.
3. The damping mechanism of an underwater Helmholtz resonator is not examined in this thesis. Instead, arbitrary damping is added to the speed of sound through air to approximate the behaviour of an underwater Helmholtz resonator.
4. The mechanical coupling of the resonators in an array, or system, of resonators is not modelled. Each resonator remains stationary within its domain and is acoustically coupled to all other resonators.
5. In chapter 6, the NMS behaviour is studied for varying air volumes, representing air loss during pile-driving. This thesis does not model air escape from the system; instead, it assumes a total percentage of lost air.

2

Literature Review

On the basis of the knowledge gap, novelty and research questions introduced in the introduction of this thesis, this chapter covers a literature review on Helmholtz resonators and acoustic metamaterials. The motivation of this literature review is to explain the principle of Helmholtz resonance and its application in Helmholtz-type acoustic metamaterials. This creates the foundation of this research.

2.1. Helmholtz Resonator

The original Helmholtz resonator was introduced in the book *On the Sensations of Tone as a Physiological Basis for the Theory of Music* by Hermann von Helmholtz in 1862 [19]. It comprises of a hollow sphere with two openings, made of glass or metal. The first opening, connected to the body of the sphere through a hollow neck, is located at the top of the sphere. On the bottom the second, larger opening is found. This device was originally developed to manipulate incoming sound at the human ear, thus being able to pick up specific frequencies and filter out unwanted frequencies.

Figure 2.1: A spherical, brass Helmholtz resonator based on the original design. Source: Physics Dept, Case Western Reserve University.

The working principle of a Helmholtz resonator is the vibration of a volume of air in the neck of the resonator. On the basis of the assumption that the diameter of the neck is much smaller than the wavelength of the incoming pressure wave [39], the Helmholtz resonator is described as a Single Degree-of-Freedom (SDoF) mass-spring system [2]. The spring stiffness is defined by the air in the cavity of the Helmholtz resonator and the mass is defined by the air in the neck of the resonator. From this, the magnitude of the mass and spring stiffness define the natural frequency of an SDoF system as $\omega_n = \sqrt{\frac{k}{m}}$. The fact that the mass of an SDoF system resonates at its natural frequency, gives a Helmholtz resonator the characteristic of interacting with incoming acoustic waves in a narrow frequency band around the natural frequency of the resonator.

Rayleigh (1916) was the first to mathematically derive the velocity potential of a spherical Helmholtz resonator, using Legendre's functions [39]. His work is based on the earlier research of Sondhauss (1850) [44], who first examined the influence of the size and shape of a resonator chamber on the resonance frequency of the resonator, and Hermann von Helmholtz (1860) [18], from which the resonator bears it's name [21]. Sondhaus (1850) found through experiments *that*

the pitch of a flask partly filled with water was not altered when the flask was inclined [44][46]. However, Alster (1972) repeated this experiments using bottles with a volume of 1 litre, and observed a clear difference in pitch *of about two tones* [2]. On this basis, he defined a new calculation of the shape dependant resonance frequency of a Helmholtz resonator.

From the definition of the natural frequency of an SDoF system, it is clearly observed that the dimensions of the Helmholtz resonator govern its natural frequency. Because of this simple characteristic, the Helmholtz resonator has been widely applied in acoustics to reduce noise in a specific narrow frequency band [9]. In the automotive industry, Helmholtz resonators are often used on automobile mufflers to reduce engine noise [58], or to mitigate tire acoustic cavity resonance (which is a significant source of vehicle interior noise) [4][38][11]. In industrial gas turbine installations, Helmholtz resonators are used to mitigate acoustic pulsations [6][53]. The sound absorption characteristics of Helmholtz resonators are even used in architectural acoustics. For instance, Helmholtz resonators are used to to provide sound absorption in a specific frequency band, or increase the transmission loss through a wall without openings [25].

More recently, the application of Helmholtz(-type) resonators in aquatic environments has been studied. Zhao et al. (2022) [60] and Rodriguez et al. (2023) [41] have published researches on the absorption of long waves by Helmholtz-type resonators in oscillating water column (OWC) structures. According to Zhao and Rodriguez, the principle of Helmholtz resonance in an OWC is analogous to the acoustic Helmholtz resonator introduced in the previous paragraphs. Zhao developed a semi-analytical model based on the potential flow theory to investigate the interaction of long waves with the OWC system. The results show that long waves can be effectively absorbed through Helmholtz resonance. Rodriguez solved a similar problem using the BEM. They show that the efficiency of the system can be greatly improved by tuning the neck parameters (e.g. the natural frequency) to the wave period of the incoming long waves. It is important to note that the long waves discussed by Zhao and Rodriguez are transverse surface waves, and that acoustic waves are longitudinal pressure waves. Nonetheless, these studies show that Helmholtz resonators can be tuned to absorb waves in specific frequency ranges.

Peng et al. (2018) published a paper on the development and modelling of a Helmholtz resonator-based NMS for offshore impact pile driving [37]. They describe the Helmholtz-type resonator as an equivalent SDoF system, of which the parameters are derived by fitting the frequency-response function of the SDoF system on the frequency-response magnitude ratio obtained from COMSOL Multiphysics. They use the BEM to determine the pressure field in a domain that is excited by a vertical array of point sources, encircled by different configurations of Helmholtz-type resonator based NMSs. It is found that the Helmholtz-type resonators are sensitive to the manually defined pressure attenuation in the air cavity of the resonator. In some cases, unwanted destructive interference at the non-target frequencies is observed. Wochner et al. conducted field tests with a panel of air-filled resonators based on the Helmholtz resonator [55]. They observed a net increase in sound pressure at frequencies below the natural frequency of the resonators. According to Wochner et al. (2016), this is due the fact that *a collective resonance of the panel is excited and the incoming sound wave can be coherently scattered* [55]. This is an important consideration, as this means that the acoustic behaviour of a Helmholtz resonator based NMS is different from the acoustic behaviour of a single Helmholtz resonator, or from the acoustic behaviour of several stand-alone Helmholtz resonators. In other words, a mechanically coupled Helmholtz resonator based NMS is excited as a whole with dynamics at low frequencies, whereas stand-alone resonators are not mechanically coupled.

An important take-away of this section is that Helmholtz resonators can absorb sound in a specific, narrow frequency range for a variety of applications. Additionally, unwanted noise amplification can, in some cases, be expected at frequencies below the natural frequency of the system.

2.2. Acoustic Metamaterials

In this section, one-dimensional arrays of evenly spaced (periodic) Helmholtz resonators are researched. Firstly, the subject of periodicity is introduced. Subsequently, two categories

of periodic materials showing unusual characteristics are introduced. Materials with such characteristics are called metamaterials and are well studied.

Acoustic waves are described as vibrations that propagate as longitudinal elastic waves. In pioneering works such as Newton's *Principia* and Rayleigh's *The Theory of Sound*, the phenomenon of periodicity is first introduced in the field of acoustics. For instance, Newton used a simple periodic mono-atomic mass-spring lattice to derive a first estimation of the speed of sound through air [8]. In other words, Newton considered a discrete system of identical (mono-atomic), evenly spread (periodic) masses connected to each other by mass-less springs. From this moment in time, numerous studies have researched phenomena originating from periodicity. A very comprehensive review on the state-of-the-art in phononic crystals and metamaterials by Hussein et al. (2014) [22], and more recently an elaborate book on elastic waves and metamaterials by Young (2023) [59], provide excellent historical and theoretical background on the subject.

2.2.1. Phononic Crystals and Bragg Scattering

Historically, as introduced in the beginning of this section, the principle of periodicity has been used to derive early approximations of nowadays widely used and accepted material characteristics. Interestingly, periodic lattices are known to have a more complex wave behaviour than original continuous media [22]. In the works of Bradley (1994) [7], and Sugimoto and Horioka (1995) [47] it is explained that wave propagation through a spatially periodic waveguide in frequency domain, known as Floquet wave propagation, can experience the formation of band gaps. A band gap is a range in the frequency domain where wave propagation is not possible, which can occur because phenomena such as Bragg scattering and local resonance. Bragg scattering is introduced in order to set the stage for the phenomenon of local resonance, which is relevant for this thesis.

In the work of Sugimoto and Horioka (1995), acoustic wave propagation in a tunnel with a periodic array of Helmholtz resonators constructed within its floor is examined. In their research, a narrow band gap is observed around the resonance frequency of the individual Helmholtz resonators, using a lumped-component approach and numerical software. Additionally, a Bragg scattering band gap is observed at a frequency of more than three times the natural frequency of the resonators. Bragg scattering occurs when the lattice constant (i.e. the spacing between individual elements) becomes a multiple of a half-wavelength,

$$d = \frac{1}{2}\lambda. \tag{2.1}$$

A material with this characteristic is called a phononic crystal. This term originates from optics where photonic crystals are a class of composite materials, which are periodic arrays of dielectric scatterers in homogeneous dielectric matrices [24]. The term crystal does not refer to the crystalline solid material, but to the lattice structure observed in these materials. The formation of band gaps as a result of Bragg scattering shows great potential in the attenuation of low frequency sound. On the basis of the work of Sugimoto and Horioka (1995), Wang and Mak (2012) show that Bragg scattering induced band gaps occur in a duct loaded with periodically spaced Helmholtz resonators, when the periodic spacing becomes a multiple of a half-wavelength (Figure 2.2a, stop-bands II). Additionally, a local resonance band gap is observed around the natural frequency of the individual resonators (Figure 2.2a, stop-band I).

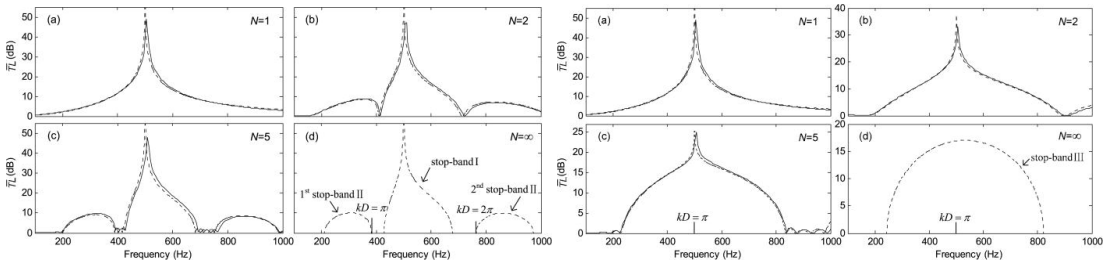

(a) Periodicity of $D = 45$ cm. **(b)** Periodicity of $D = 34.4$ cm.

Figure 2.2: Transmission loss in a duct with N resonators, analytical (dotted lines) and numerical (solid lines) predictions [54].

Finally, they show a third, broader, band gap type around the natural frequency of the resonator (Figure 2.2b, stop-band III). This band gap shows the combined effects of a Bragg scattering band gap and a local resonance band gap, where the frequency range of the local resonance is governing and the shape of the Bragg scattering band gap is adopted. This shows promising applications for situations with high frequencies, where the wavelengths are small (or situations where the order of magnitude of the dimensions of the metamaterial is not an issue). In the offshore installation environment, NMSs with dimensions in the order of magnitude of the wavelength of impact pile driving noise is unfortunately not practical. This makes phononic crystals unsuitable for the application in NMSs for offshore impact pile driving. However, the effect of local resonance shows promising possibilities for NMSs for offshore impact pile driving. This phenomenon is discussed in the next paragraphs.

2.2.2. Acoustic Metamaterials and Local Resonance

In the previous section, it is introduced that the lattice constant or periodicity of a phononic crystal has to be in the order of magnitude off the target wavelength to be effective. Because of this, phononic crystals are mainly used in the ultrasonic regime [28]. Locally resonant metamaterials can resolve this problem, as well as introduce characteristics that are usually not observed in ordinary composites. The resonance frequency of a unit cell of a locally resonant metamaterial depends on the inertia and the restoring force of the system [28]. Therefore, the resonance frequency can be tuned to an arbitrary magnitude. In other words, the dimensions of the unit cells can be orders of magnitude smaller than the wavelength. Consequently, the effective medium approximation is valid [13].

The effective medium theory describes the macroscopic properties of advanced composite materials. In materials science, advanced composite materials are materials that are characterised by unusually high stiffness or elasticity, while bound together by weaker matrices compared to their conventional counterparts. These sub-wavelength characteristics are a common feature in different types of metamaterials. In acoustic metamaterials, these unusual characteristics occur in the form of negative (or zero valued) effective acoustic properties [59][22]. For instance, a negative bulk modulus implies that volume change is out of phase with applied dynamic pressure, and negative mass density implies that acceleration is out of phase with the dynamic pressure gradient [13]. Because these properties induce out-of-phase behaviour, energy of a propagating wave can be decreased. In the unit cells of locally resonant acoustic metamaterials, these characteristics occur in a narrow band around the resonance frequency of the unit cell. Consequently, band gap formation can be observed around the resonance frequency of the unit cells. These sub-wavelength characteristics are promising for offshore applications, as the wavelengths of the pressure waves radiated during offshore impact pile driving are large. Additionally, acoustic metamaterials *are useful in manipulating acoustic waves that are governed by Newton's law of motion, the fluid continuity equation, and the thermodynamic equation of state (for adiabatic process)*, according to Ma and Sheng (2016) [28].

Similarly to the unit cell of a locally resonant metamaterial, a Helmholtz resonator can achieve narrow banded noise attenuation at an arbitrarily low frequency range (section 2.1). Liu and Yang (2017) describe that a periodically mounted array of Helmholtz resonators can facilitate

absorption in a broader frequency range, compared to the narrow frequency range at which a single Helmholtz resonator acts [27]. In their work, one narrow attenuation range is observed for a system with a single Helmholtz resonator (Figure 2.3a, pink graph). However, for a system with four periodically spaced Helmholtz resonators, two broad attenuation ranges are observed (Figure 2.3a, blue and black graphs). One band gap is formed in a broad frequency range around the natural frequency of the individual resonators, and the other band gap begins at a frequency where the lattice constant is equal to half the wavelength. Additionally, the acoustic band structure of an ideal periodic seawater pipe system shows exactly the same attenuation ranges as the system with four periodically spaced Helmholtz resonators (Figure 2.3b). An interesting observation is that the band gap resulting from the local resonance of the array of resonators is significantly broader than the attenuation range of a single resonator. Moreover, this band gap is not the result of thermo-viscous losses in the Helmholtz resonators, e.g., it also occurs in a lossless case. This shows that Helmholtz-type locally resonant metamaterials can realise the formation of broad band gaps around the natural frequency of a single Helmholtz resonator (e.g. unit cell).

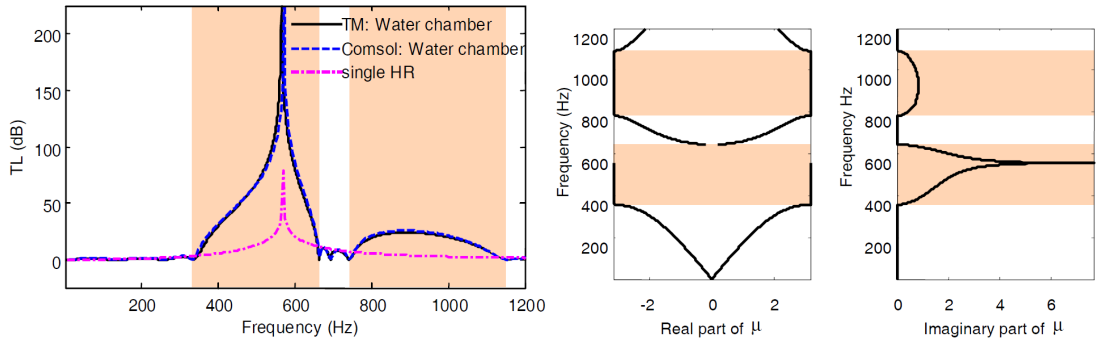

(a) Array of four Helmholtz resonators

(b) Infinite array of Helmholtz resonators

Figure 2.3: Local Resonance and Bragg scattering: band gap formation from Helmholtz resonators in a seawater piping system [27].

According to Liu and Yang, the principle of a Helmholtz-type locally resonant metamaterial rests on two conditions:

1. If an array of Helmholtz resonators is configured periodically with a lattice constant much smaller than the acoustic wavelength, the periodic system will behave as a homogenised effective medium where a band gap is expected.
2. If the dimensions of a Helmholtz resonator are much smaller than the acoustic wavelength, the Helmholtz-resonator can be defined as a local resonator.

These conditions are very similar to the condition regarding the effective medium approximation discussed in the beginning of this subsection, and are used to check the validity of an underwater Helmholtz-type metamaterial.

2.2.3. Functionally Graded Metamaterials

Functionally Graded Materials (FGMs) represent a sophisticated category within the broader family of engineering composites, characterised by the integration of two or more constituent phases that exhibit a continuous and smooth variation in composition. The distinctiveness of these advanced materials lies in their engineered gradients of composition, structure, and/or specific properties, which are oriented in a preferred direction. This unique configuration makes these materials better than similar materials with a homogeneous composition.

In materials engineering, FGMs have been widely used to give homogeneous metamaterials an additional or a broader stop band. For instance, Pedersen et al. (1982) published a paper on the impedance matching properties of an inhomogeneous matching layer [36]. They studied the performance of the matching layer for varying characteristics, such as sound speed and density,

and found the transmission and reflection properties. The inhomogeneous matching layer is configured with an exponential profile. Similarly to Pedersen, Sepehri et al. (2020) investigated structures made of FGMs with an exponential profile and the effect of the functional grading on the band gap formation in elastic wave propagation [43]. They found that FGMs show a higher percentage of band gaps and that these characteristics can be tuned to a specific application by changing specific characteristics.

Thus far, functional grading has been mainly used in material science by gradually changing specific material properties in a solid, in order to realise behaviour that a homogeneous material can not show. In order to gain insight on what impact functional grading can have in other applications, it is interesting to research this phenomenon in the application of discrete acoustic metamaterials.

2.3. Conclusion

Helmholtz resonators are capable of interacting with sound at a frequency coinciding with its natural frequency, which is based on the geometry of the resonator. Studies show that, because of this characteristic, Helmholtz resonators are easy to tune and subsequently applied to mitigate noise in very specific frequency ranges. The downside of Helmholtz resonators is that the noise mitigation occurs always in a narrow frequency band.

Metamaterials show characteristics that the conventional materials of which they are built up of can not show. In acoustics, metamaterials are used in the form of phononic crystals and locally resonant acoustic metamaterials to introduce broadband noise attenuation. It is noted that phononic crystals are not suitable in the application of NMSs for offshore impact pile driving, because their geometry is related to the target wavelength. In contrast, locally resonant metamaterials work in sub-wavelength configurations. Locally resonant acoustic metamaterials exist in the form of arrays of Helmholtz resonators, where the limiting narrow band characteristics of Helmholtz resonators are resolved. This shows large potential for the mitigation of low-frequency noise emitted during offshore impact pile driving. Additionally, functional grading is sometimes applied to metamaterials. Studies show that FGMs show better characteristics than their homogeneous counterpart.

In the next chapters, the large potential of the application of locally resonant metamaterials in Helmholtz-type NMSs for offshore impact pile driving is investigated. The setup of the BEM and the FEM models are introduced in chapter 3, after which these are applied to define the characteristics of a reference resonator and to investigate the behaviour of a periodic Helmholtz-type NMS.

3

Solution Method and Model Setup

In this chapter, the method used to solve the acoustic wave equation is introduced. Subsequently, the model setup of the BEM and FEM in different coordinate systems are discussed.

3.1. Solution Method

The acoustic wave equation in a homogeneous medium without a source is given by

$$\nabla^2 p(t) - \frac{1}{c^2}\frac{\partial^2 p(t)}{\partial t^2} = 0, \tag{3.1}$$

where ∇^2 is the Laplace operator, p is the acoustic pressure, t is the time and c is the speed of sound through the medium. Equation 3.1 is in the time domain, however, problems in ocean acoustics are often solved in the frequency domain. The primary advantage is that in the frequency domain, an ordinary differential equation is solved. In contrast, in the time domain, a partial differential equation is solved, which requires more computational power [23]. Therefore, the frequency-time Fourier transform pair is used to obtain the frequency-domain acoustic wave equation, or the homogeneous Helmholtz equation. A source term is easily included in the right-hand side of the equation, resulting in the inhomogeneous Helmholtz equation

$$\left[\nabla^2 + k(\omega)^2\right] p(\omega) = f(\omega). \tag{3.2}$$

Here, ω is the angular frequency, $k(\omega)$ is the wave number and $f(\omega)$ is the forcing term. An inhomogeneous linear differential equation, such as Equation 3.2, is satisfied by a Green's function if the right-hand-side is an impulse. Therefore, the Green's function satisfies the inhomogeneous Helmholtz equation as follows

$$\left[\nabla^2 + k(\omega)^2\right] G_\omega(\mathbf{r}, \mathbf{r}_0) = -\delta(\mathbf{r} - \mathbf{r}_0), \tag{3.3}$$

where $[\nabla^2 + k(\omega)^2]$ is the linear differential operator, $\mathbf{r}$ is any location in the field, $\mathbf{r}_0$ is the location of the source and δ is the Dirac delta function defining a unit impulse (this is important for the validity of the Green's function, discussed in Appendix A). A general Green's function is introduced by Jensen (2011), which comprises of a particular solution $g_\omega(\mathbf{r}, \mathbf{r}_0)$ and a homogeneous solution $H_\omega(\mathbf{r})$:

$$G_\omega(\mathbf{r}, \mathbf{r}_0) = g_\omega(\mathbf{r}, \mathbf{r}_0) + H_\omega(\mathbf{r}), \tag{3.4}$$

where $H_\omega(\mathbf{r})$ is any function that satisfies the homogeneous Helmholtz equation and $g_\omega(\mathbf{r}, \mathbf{r}_0)$ is any function that satisfies the radiation condition [23]. A substitution of the two solutions satisfies the boundary conditions and the radiation condition.

A semi-analytical method for solving problems in which Green's functions are calculated, is the Boundary Element Method (BEM). The BEM is a computational method for solving linear

partial differential equations which are formulated as integral equations. Jensen et al. (2011) [23] introduced the solution of the inhomogeneous Helmholtz equation in a bounded medium as

$$p(\mathbf{r},\omega)=\int_S\left[G_\omega\left(\mathbf{r},\mathbf{r}_0\right)\frac{\partial p\left(\mathbf{r}_0\right)}{\partial\mathbf{n}_0}-p\left(\mathbf{r}_0\right)\frac{\partial G_\omega\left(\mathbf{r},\mathbf{r}_0\right)}{\partial\mathbf{n}_0}\right]dS_0-\int_V f\left(\mathbf{r}_0\right)G_\omega\left(\mathbf{r},\mathbf{r}_0\right)dV_0, \tag{3.5}$$

where $\mathbf{n}_0$ is the outward-pointing normal on any surface S_0 inside the domain, and V_0 is the volume of the source.

3.2. Model Setup: BEM

In this section, the application of the BEM in two different coordinate systems is discussed. Firstly, the Green's function and boundary integral formulation for a one-dimensional model are introduced. Secondly, the Green's function and boundary integral formulation for a two-dimensional model are introduced.

3.2.1. One-Dimensional System

In chapter 2, the phenomenon of periodicity in structures is introduced. To study periodic effects in Helmholtz-type NMSs, a horizontal array of Helmholtz-type resonators is introduced to an infinite domain. The domain is excited by a point source centred at the origin of the domain. In an infinite domain the system is conveniently described in spherical coordinates ($\mathbf{r}=r,\theta,\phi$), in which the propagation of the pressure wave and the location of each resonator only depends on the range r from the source. Therefore, this system becomes one-dimensional in the r-direction ($\mathbf{r}=r,0,0$). Correspondingly, the Laplace operator is

$$\nabla^2=\frac{1}{r^2}\frac{\partial}{\partial r}r^2\frac{\partial}{\partial r}. \tag{3.6}$$

As discussed in the beginning of this chapter, the Green's function satisfies the Helmholtz equation (Equation 3.3). In an infinite domain there exist no boundary conditions, i.e., the system must only satisfy the radiation condition at $r=\infty$. Therefore, the Green's function only comprises of a particular solution (the homogeneous solution is equal to zero and therefore omitted). For a point source in an infinite domain, the Green's function is defined by Jensen et al. (2011) [23] as

$$g_\omega(\mathbf{r},\mathbf{r}_0)=\frac{e^{ik|\mathbf{r}-\mathbf{r}_0|}}{4\pi|\mathbf{r}-\mathbf{r}_0|}, \tag{3.7}$$

where k is the medium wave number, $\mathbf{r}_0$ is the location of the source and $\mathbf{r}$ is any range in the field. The Green's function is then included in the boundary integral formulation introduced in the previous section, resulting in the boundary integral for a point source in an infinite domain. Peng et al. (2018) introduced a method to include underwater Helmholtz-type resonators to the boundary integral formulation, to consider their effect on the resulting pressure field [37]. The resonators are included as surfaces in the first integral of Equation 3.8, and their effect on the pressure field is included through their frequency response function. In order to realise this, the pressure at the centre point of each resonator must be determined. In Equation 3.8, the location of the point $\mathbf{r}$ in the field is replaced by the location of the centre point of each resonator $\mathbf{r}_R$ as $\mathbf{r}=\mathbf{r}_m^R$. This results in a linear system which is solved for the pressure $\tilde{p}(\mathbf{r}_m^R,\omega)$ at the centre of each resonator. The full derivation of the linear system is included in Appendix C. Subsequently, the pressure $\tilde{p}(\mathbf{r}_m^R,\omega)$ is reintroduced in the boundary integral formulation, resulting in the final pressure field.

$$\tilde{p}(\mathbf{r},\omega)=\sum_{m=1}^{M}\left\{\int_S\left[g_\omega\left(\mathbf{r},\mathbf{r}_m^R\right)\frac{\partial\tilde{p}\left(\mathbf{r}_m^R\right)}{\partial\mathbf{n}_0}-\tilde{p}\left(\mathbf{r}_m^R\right)\frac{\partial g_\omega\left(\mathbf{r},\mathbf{r}_m^R\right)}{\partial\mathbf{n}_0}\right]dS_0\right\}-\int_V f(\mathbf{r}_0)g_\omega(\mathbf{r},\mathbf{r}_0)dV_0, \tag{3.8}$$

where the first integral is solved for each resonator r_m^R, resulting in M solutions. These solutions are then summed to obtain the coupled pressure response of the system of resonators.

3.2.2. Two-dimensional System

In offshore activities such as monopile installation for offshore wind turbines, the pressure field produced during impact pile driving is best described in a cylindrical coordinate system. This is convenient because the pressure field can be assumed to be axisymmetric around the z-axis, reducing it to a plane. In this case, the Laplace operator is

$$\nabla^2 = \frac{1}{r}\frac{\partial}{\partial r} r \frac{\partial}{\partial r} + \frac{\partial^2}{\partial z^2}. \tag{3.9}$$

From the equation above it is observed that the system is two-dimensional, dependent on the range r and the depth z. A numerically attractive method for solving the Helmholtz equation in a two-dimensional cylindrical coordinate system is the normal mode method. The normal mode method assumes that the pressure field can be decomposed into a sum of normal modes. These modes are similar to the modes of a vibrating string, where mode m is a sine wave with m anti-nodes and $m+1$ nodes. The pressure field is then constructed by summing the contributions of each mode. The contribution of each mode is determined by the dispersion relation, which relates the mode's frequency to its horizontal wavenumber (Equation 3.10). Solving the Helmholtz equation leads to an eigenvalue problem, where the modes are characterised by an eigenfunction (mode shape function) and an eigenvalue (horizontal wavenumber). On the basis of the boundary conditions, the vertical wavenumber is also derived (Equation 3.11). This solution process is clearly documented in *Computational Ocean Acoustics* by Jensen et al. (2011) [23], and is included in Appendix B.

$$k_r = \sqrt{\left(\frac{\omega}{c}\right)^2 - \left[\left(m - \frac{1}{2}\right)\frac{\pi}{D}\right]^2} \tag{3.10}$$

$$k_z = \sqrt{\left(\frac{\omega}{c}\right)^2 - k_r^2} \tag{3.11}$$

Similar to the one-dimensional model, the Green's function satisfies the inhomogeneous Helmholtz equation. The main difference is that this domain is bound at the seabed and the sea surface, in addition to the radiation condition. For simplicity, the seabed is described by a rigid boundary condition where the velocity is equal to zero

$$\tilde{v}_z(r, z_D, \omega) = 0, \tag{3.12}$$

$$\frac{\partial \tilde{\phi}}{\partial z_D} = 0. \tag{3.13}$$

The sea surface is described by a pressure release boundary where the pressure is equal to zero, because the impedance difference between the seawater and atmosphere is large

$$\tilde{p}(r, z_0, \omega) = 0, \tag{3.14}$$

$$\tilde{\phi}(r, z_0, \omega) = 0, \tag{3.15}$$

$$\tilde{\psi}(r, z_0, \omega) = 0. \tag{3.16}$$

From this, the Green's function is obtained from Jensen et al. (2011) [23] and Peng et al. (2018) [37]

$$G_\omega(\mathbf{r}, \mathbf{r}_0) = \sum_{m=1}^{\infty} \left[\frac{i}{2D} sin(k_z z_0) sin(k_z z) H_0^{(1)}(k_r r')\right], \tag{3.17}$$

where D is the water depth, $\mathbf{r}$ is the location of a point in the field with respect to the source location $\mathbf{r}_0$ and m is the mode number. $H_0^{(1)}(k_r r')$ is the Hankel function of the first kind, used to express the propagation of the waves resulting from the cylindrical wave equation. In this thesis, the Hankel function of the first kind is used, because the positive value of the horizontal wave number is used (Appendix B).

The Green's function for a bounded domain is then included in the boundary integral formulation (Equation 3.5), resulting in the boundary integral for an point source in a bounded domain

$$\tilde{p}(\mathbf{r},\omega) = \sum_{m=1}^{M} \left\{ \int_S \left[G_\omega\left(\mathbf{r},\mathbf{r}_m^R\right) \frac{\partial \tilde{p}\left(\mathbf{r}_m^R\right)}{\partial \mathbf{n}_0} - \tilde{p}\left(\mathbf{r}_m^R\right) \frac{\partial G_\omega\left(\mathbf{r},\mathbf{r}_m^R\right)}{\partial \mathbf{n}_0} \right] dS_0 \right\} - \int_V f(\mathbf{r}_0) G_\omega(\mathbf{r},\mathbf{r}_0) dV_0. \quad (3.18)$$

Similar to the boundary integral formulation of an infinite domain, the first integral is solved for each resonator r_m^R and summed over M solutions. The method to derive the pressure at the open end of each resonator is the same as for the one-dimensional model. In summary, the location of the field point is replaced by the location of the centre point of each resonator $\mathbf{r}_R$. The resulting linear system is then solved for the pressure $p(\mathbf{r}_R,\omega)$. In the next subsection, the setup of the model in COMSOL Multiphysics is discussed.

3.3. Model Setup: FEM

In this thesis, the *Pressure Acoustics* package of the Acoustic Module of COMSOL Multiphysics (CM) is used to solve the Helmholtz equation with the FEM. Similar to the BEM models, an infinite domain and a bounded domain are created.

3.3.1. Geometry

In section 3.2, it is discussed that the propagation of a pressure wave radiated by a point source in an infinite domain is conveniently described in a spherical coordinate system. In CM, a domain is created by introducing a geometry into a coordinate system. For convenience, a sphere is created (Figure 3.1a). Additionally, a point geometry is included at the location of the source (e.g. the origin). Finally, the underwater Helmholtz-type resonator is included as two connected cylinders. One cylinder represents the air cavity in the resonator and the other cylinder represents the water column in the resonator (Figure 3.1c).

Similarly, a bounded domain is created by means of a cylindrical geometry (Figure 3.1b). A point geometry is included at half the height of the cylinder and the resonator (arrays) is (are) included at $r = 2$ m from the point geometry.

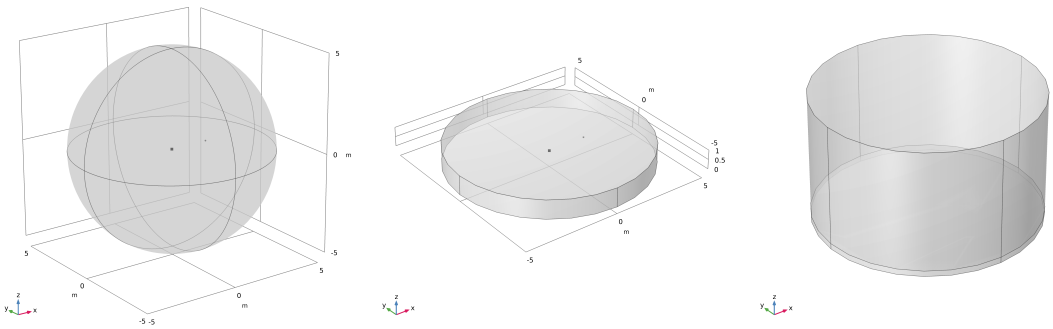

(a) One-dimensional spherical geometry **(b)** Two-dimensional cylindrical geometry **(c)** Underwater Helmholtz-type resonator

Figure 3.1: Images of the spherical and cylindrical domain, and the Helmholtz-type resonator.

3.3.2. System Parameters and Boundary Conditions

The seawater and the air inside the resonator are specified as linear elastic fluids. That is, no losses are initially included. Defining the sound attenuation of a Helmholtz-type resonator is a difficult task and is not within the scope of this thesis, as discussed in chapter 1. Therefore, the damping inside the Helmholtz-type resonator is included by adding an imaginary part to the speed of sound through air as

$$c = c_r + ic_i. \quad (3.19)$$

The properties of the fluids are listed in Table 3.1.

General	
Temperature	283 K
Background pressure	101325 Pa
Water	
Speed of sound	1490 m/s
Density	1025 kg/m^3
Air	
Speed of sound	337 m/s
Density	1.25 kg/m^3

Table 3.1: User-defined system parameters.

A point source is included in CM by specifying the physics of a monopole point source on the point geometry introduced in the previous paragraph. The source strength is defined as a monopole amplitude and set to $S = 1$ N/m. This source yields a pressure amplitude of unity at $r = 1$ m.

In the bounded model, the rigid boundary at the seabed is modelled as a *Sound Hard Boundary*. That is, the normal component of the acceleration (e.g. the velocity) at the boundary is zero. Additionally, a *Sound Soft Boundary* is included at the sea surface. Here, the pressure equals zero at the boundary. Recall that the same boundary conditions are included in the BEM model. In both the infinite and bounded models the radiation condition is included as a *Perfectly Matched Boundary*, which is analogous to a fully permeable radiation condition.

The shell of the Helmholtz-type resonators are specified as *Interior Sound Hard Boundary*. Similar to the *Sound Hard Boundary*, the boundary is fully reflective and the normal component of the acceleration is zero at the shell.

3.3.3. Meshing

In CM, the meshing can be done manually, or automatically through the physics-controlled mesh for pressure acoustics. The physics-controlled mesh is based on the frequency range of the study. It appropriately defines the meshing, based on the maximum frequency defined in the frequency step. The default value is set to 5 nodes per wavelength, however, this is increased to six to create a slightly finer mesh. The mesh will automatically be different for the resonator and the rest of the domain as the speed of sound through air is different than the speed of sound through water, resulting in a more efficient model. The mesh automatically resolves the wave and the perfectly matched boundaries are appropriately meshed [32]. The resulting meshes are depicted in Figure 3.2.

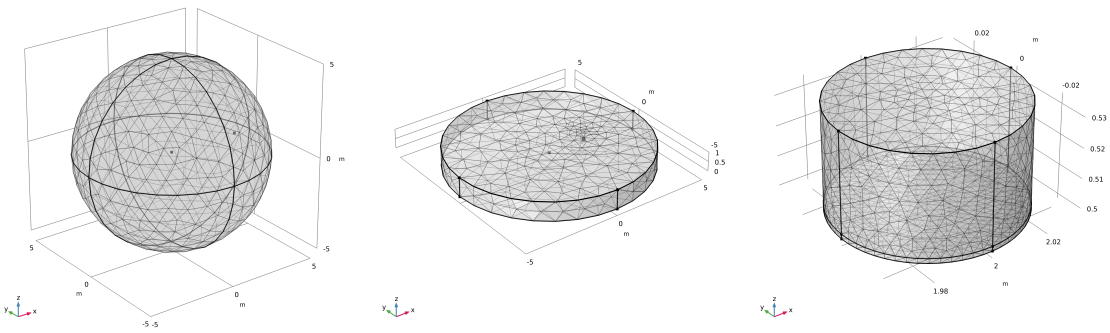

(a) One-dimensional spherical geometry mesh

(b) Two-dimensional cylindrical geometry mesh

(c) Underwater Helmholtz-type resonator mesh

Figure 3.2: Images of the meshing of the spherical and cylindrical domain, and the Helmholtz-type resonator.

In the next chapter, the Helmholtz-type resonator is defined using the lumped-component

approach. The mass, spring stiffness and damping ratio are defined by using the pressure at the open end of the resonator and the lumped-component equation of motion to define the frequency-response magnitude ratio of the resonator.

4

Defining the Resonator Characteristics

In this chapter, the characteristics of a reference Helmholtz-type resonator are defined. The resonator is cylinder-shaped, with an open end at the bottom flat side. The height L of the resonator is 0.035 meter and the radius is 0.03 meter. As discussed in the previous section, the walls of the resonator are assumed to be rigid. Firstly, the frequency response function of the reference resonator is defined. Thereafter, spring stiffness and damping ratio are obtained through the lumped-component approach.

It is important to recall that the main working principle of a Helmholtz resonator is the vibration of a fluid in the neck of the resonator. Figure 4.1 shows the vertical cross section of the reference resonator, schematised as a lumped-component system. The resonating mass is represented by the volume of water V_w pushed inside the resonator through hydrostatic pressure, and the volume of air V_a trapped between the rigid walls of the resonator and V_w represents the air-filled cavity.

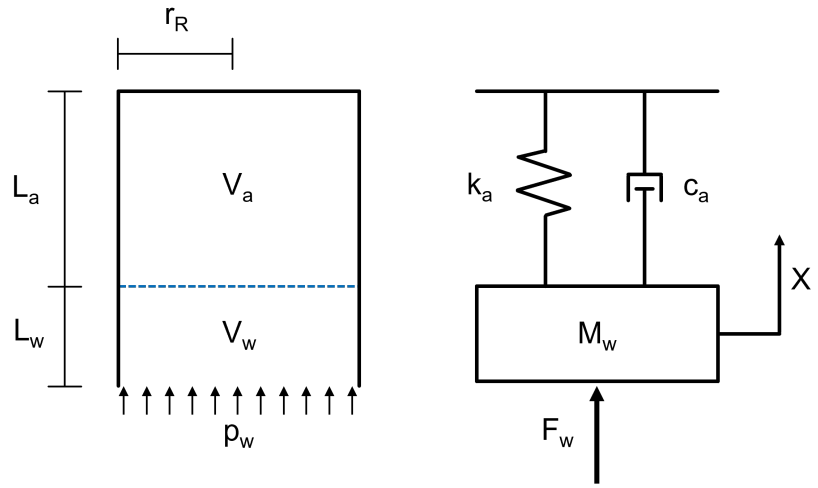

Figure 4.1: Lumped-component model of a Helmholtz-type resonator, describing a unit cell of a Helmholtz-type acoustic metamaterial.

Similar to the SDoF mass-spring system of the original Helmholtz resonator, Newton's second law of motion is conveniently used on a SDoF mass-spring-damper system analogous to the Helmholtz-type resonator [57][42][9]. Additionally, it is assumed that the wavelengths of the

incoming acoustic pressure waves are much larger than the diameter of the open end of the underwater Helmholtz-type resonator. The assumption is checked for the highest frequency used in this study (300 Hz), as this results in the smallest wavelength. Equation 4.1 shows that the assumption is valid.

$$\lambda = \frac{c}{f} = \frac{1490}{300} = 4.97m, \quad 4.97m >> 0.06m \tag{4.1}$$

From this, the pressure p_w over the area of the open end is constant, subsequently providing the force F_w that excites the mass-spring-damper system. The equation of motion is expressed as

$$\frac{\partial^2 X(t)}{\partial t^2} + 2\zeta\omega_n \frac{\partial X(t)}{\partial t} + \omega_n^2 X(t) = \frac{\omega_n^2}{k} F_w(t) \tag{4.2}$$

where $\omega_n = \sqrt{\frac{k_a}{m_w}}$ and $\zeta = \frac{c_a}{2\sqrt{m_w k_a}}$, which are both unknowns. In order to study the dynamic behaviour of an underwater Helmholtz-type resonator, the frequency response function has to be defined.

Firstly, the displacement amplitude of the volume of water has to be derived. Based on the assumption that the volume of air in the resonator fluctuates when it is excited by an acoustic pressure wave, the displacement amplitude of the volume of water can be obtained. In subsection 2.2.2, it is stated that acoustic metamaterials are useful in manipulating acoustic waves that are governed by the thermodynamic equation of state for adiabatic processes. Therefore, the ideal gas law for a gas undergoing a reversible adiabatic process is considered

$$PV^\gamma = constant, \tag{4.3}$$

where γ is the adiabatic index, which is equal to $\frac{7}{5}$ for diatomic gasses. For the purpose of this thesis, this law is rewritten in the following form

$$P_1 V_1^\gamma = P_2 V_2^\gamma. \tag{4.4}$$

Secondly, let us recall that the mass in the lumped-component model (Figure 4.1) is a point mass specified by the volume of the water column inside the resonator. Therefore, the displacement X of the point mass is directly proportional to the change in volume of the air inside the resonator. Because of this, Equation 4.4 is reformulated into

$$P_1 V_1^\gamma = P_2 (V_1 - |X(\omega)| A_r)^\gamma \tag{4.5}$$

where $|X(\omega)|$ and A_r are the absolute displacement of the point mass and the area of the open end of the Helmholtz-type resonator. P_1 is the hydrostatic pressure, V_1 is the initial volume of the air pocket and P_2 is the pressure in the new state at the air-water interface inside the Helmholtz-type resonator. In an unforced environment, P_2 is equal to P_1 and is easily calculated using

$$P_2 = P_0 + \rho_w g z \tag{4.6}$$

where P_0 is the atmospheric pressure at the sea surface, g is the gravitational acceleration and z is the depth of the resonator. In the case of a forced environment, P_2 is obtained using the FEM model introduced in the previous chapter. For the reference Helmholtz-type resonator at a depth of $z = 0.5$ m, the real and imaginary part of the pressure at the air-water interface in the resonator are depicted. The complex pressure is split into its real and imaginary part in order to showcase the damping included in FEM, as explained in section 3.3.

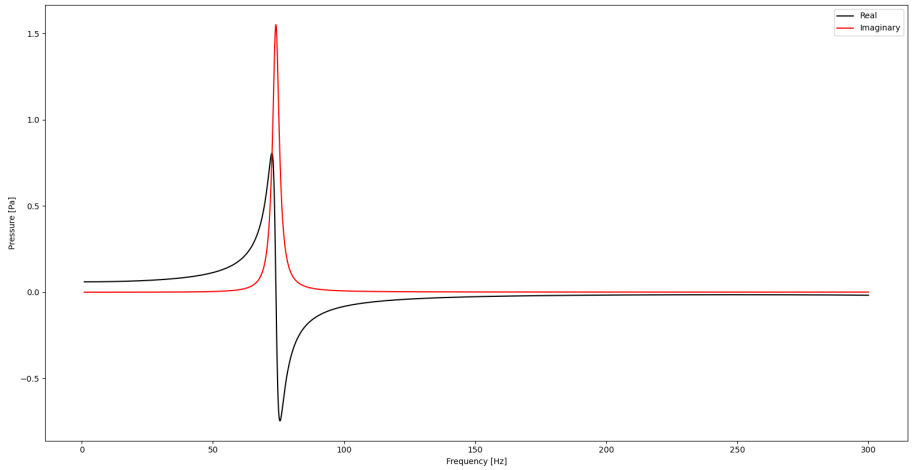

Figure 4.2: Pressure at the open end of an underwater Helmholtz-type resonator with radius $r = 0.03$ m and height $L = 0.035$ m, at a water depth of $z = 0.5$ m.

Equation 4.2 is transformed into the frequency domain by use of the Fourier transform, after which the frequency-response magnitude ratio is written in the form of the dynamic flexibility

$$\left|\frac{X(\omega)}{X(0)}\right| = \frac{1}{\sqrt{\left(1 - \frac{\omega^2}{\omega_n^2}\right)^2 + 4\xi^2\frac{\omega^2}{\omega_n^2}}} \tag{4.7}$$

where $X(0)$ is the static displacement for $\omega \to 0$. As mentioned in the beginning of this chapter, ω_n, k and ξ are unknown. To solve for the unknowns, the pressure P_2 from Figure 4.2 is inserted into Equation 4.5, which is solved for the displacement amplitude $X(\omega)$. The frequency-response magnitude ratio is then plotted and curve-fitted for the right-hand-side of Equation 4.7 using a least-squares curve-fitting tool, this is depicted in Figure 4.3. The resulting resonator characteristics are listed in Table 4.1.

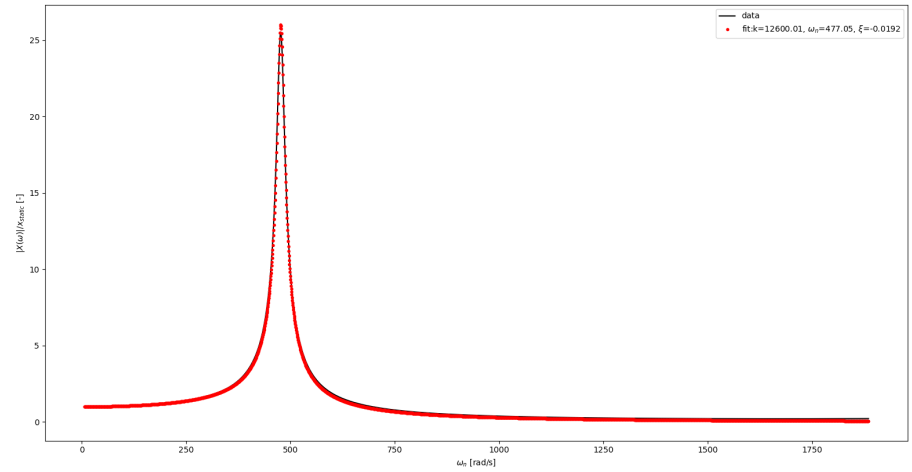

Figure 4.3: Frequency-response magnitude ratio of the volume of water inside an underwater Helmholtz-type resonator with radius $r = 0.03$ m and height $L = 0.035$ m, at a water depth of $z = 0.5$ m.

Natural frequency	ω	477.05 rad/s
Spring stiffness	k	12600.01 N/m
Damping ratio	ξ	0.0192

Table 4.1: Characteristics of an underwater Helmholtz-type resonator with radius $r = 0.03$ m and height $L = 0.035$ m, at a water depth of $z = 0.5$ m.

Similarly, this method is used to determine the frequency response function for different water depths. For this, the relationship between the hydrostatic pressure and the mass of the water column inside the resonator is required. The length of the water column L_w is described as

$$L_w = \frac{V_r - V_a}{A_r}, \tag{4.8}$$

where V_r and A_r are the volume of the resonator and the area of the open end of the resonator, respectively. In correspondence with the ideal gas law, the volume of air inside the resonator is described as

$$V_a = \frac{m_a}{\rho_a} = \frac{m_a V_r R T}{P_0}, \tag{4.9}$$

where m_a and ρ_a are the mass and density of the air inside the resonator in dry conditions, R is the specific gas constant, T is the temperature and P_0 is the hydrostatic pressure. By combining Equation 4.8 and Equation 4.9, it is derived that the length of the water column inside the resonator is described as

$$L_w = \frac{V_r}{A_w}\left(1 - \frac{\rho_a R T}{P_0}\right). \tag{4.10}$$

From L_w, the depth dependent volumes V_1 and V_2 are determined. The results are plotted in Figure 4.4 for three cases. Firstly, it is assumed that the mass of the air inside the resonator is equal to the mass of the air inside the resonator when the system is in-air. Secondly, a reduction of 30% of air is considered. Finally, a reduction of 70% of air is considered. The effect of the reduction of air on the noise attenuation of a Helmholtz-type NMS is discussed in chapter 6.

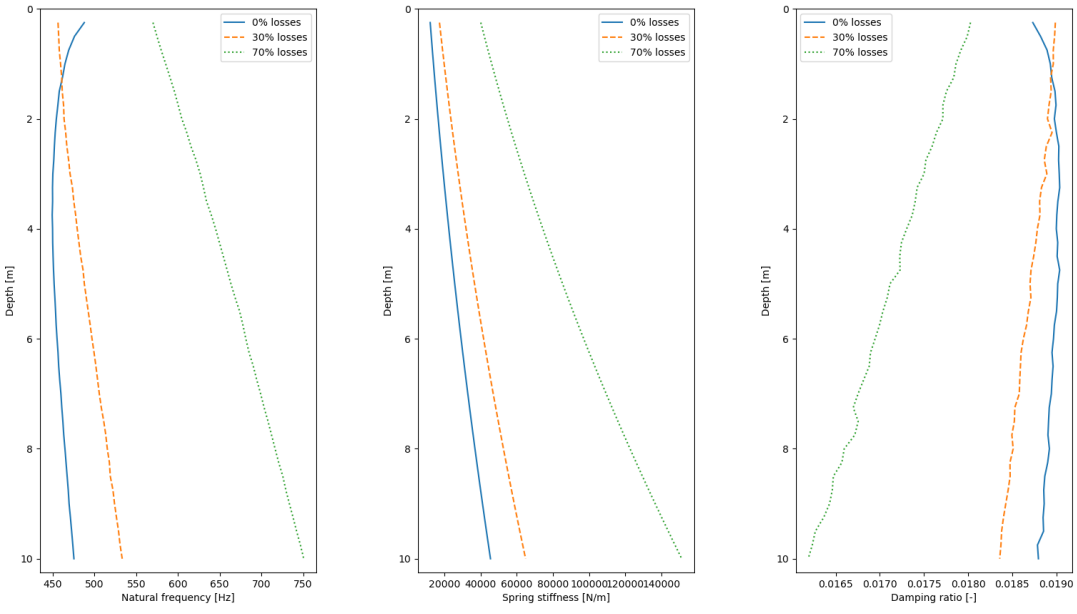

(a) Natural frequency **(b)** Spring stiffness **(c)** Damping ratio

Figure 4.4: Resonator characteristics of a resonator with radius $r = 0.03$ m and height $L = 0.035$ m, for depths between $z = 0.25$ m and $z = 10$ m.

To understand how the natural frequency, spring stiffness and damping ratio change if part of the trapped air is lost, the lumped-component approach must be recalled. From this, the definition of the spring stiffness is

$$k_a = \frac{P_S A_r}{X(0)}, \tag{4.11}$$

where, P_S is the static pressure at the open end of the resonator at $\omega \to 0$, A_r is the cross sectional area of the resonator and $X(0)$ is the static displacement at $\omega \to 0$. Hence, the spring stiffness is inversely proportional to the volume of trapped air. Because P_S and A_r remain constant, the spring stiffness increases when the volume of trapped air decreases. From this, the spring stiffness and the lumped mass define the natural frequency ω_n as

$$\omega_n = \sqrt{\frac{k_a}{M_w}} \tag{4.12}$$

where k_a is the spring stiffness and M_w is the mass of the water inside the resonator. Both k_a and M_w increase when trapped air is lost. However, the increase in spring stiffness is larger than the increase in mass, because the air volume change impacts the spring stiffness due to its inverse proportionality, whereas the same volume change results in a relatively small increase in mass. From this, it is expected that the natural frequency increases. Finally, the damping ratio is defined as

$$\xi = \frac{c_a}{2\sqrt{M_w k_a}}, \tag{4.13}$$

where c_a is the damping coefficient. While the spring stiffness and the lumped mass increase, it is assumed that the damping coefficient remains constant. Therefore, the damping ratio decreases. The influence of the varying lumped-component characteristics on the noise attenuation of the Helmholtz-type NMS is investigated in the following section.

5

Periodic Systems of Helmholtz-type Acoustic Metamaterials

In the previous chapters, the model setup is discussed and the depth-dependent characteristics of the reference Helmholtz-type resonator are defined. In this chapter, the influence of periodicity on the noise attenuation of various systems of Helmholtz-type resonators is studied. In section 5.1, the influence of periodicity on a horizontal array of Helmholtz-type resonators, henceforth called a Helmholtz-type acoustic metamaterial, is studied. On the basis of the findings from section 5.1, the influence of periodicity on a vertical system of Helmholtz-type acoustic metamaterials is studied in section 5.2.

5.1. Helmholtz-type Acoustic Metamaterial

In the literature review (chapter 2), the application of Helmholtz(-type) resonators in acoustic metamaterials is introduced. Results from several studies show that broadband attenuation can be realised when acoustic metamaterials are tuned to a specific configuration. Therefore, this section studies the sensitivity of the number of resonators, the distance between the individual resonators and the type of grading of the array, on the sound pressure attenuation of a Helmholtz-type acoustic metamaterial.

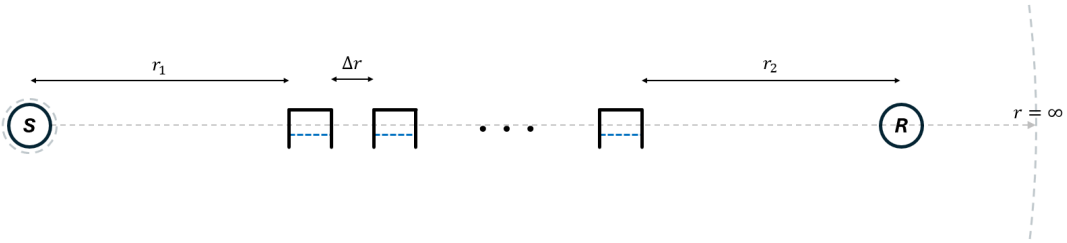

Figure 5.1: Helmholtz-type acoustic metamaterial in an infinite domain excited by a point source. A spherical radiation condition is considered.

The Helmholtz-type acoustic metamaterial is modelled in the infinite domain introduced in subsection 3.2.1, of which a schematisation is included in Figure 5.1. The source S is located at the origin of the domain and the receiver is located at a distance of $r_1 + N \cdot \Delta r + r_2$ from the source, where N is the number of resonators within the Helmholtz-type acoustic metamaterial. The parameters that define the geometry of the system above are listed in Table 5.1. The value for r_1 is based on an approximation of the difference in radius of a monopile and a near-pile NMS. Additionally, the value of r_2 in the main study is based on a study considering the sensitivity of the distance between the final resonator in the array and the receiver (Appendix D).

[m]	Validation	Main study
r_1	2	2
Δr	-	0.05, 0.1, 0.5, 1, 5
r_2	2	$229 - r_1 - (N \cdot \Delta r)$

Table 5.1: System parameters for a Helmholtz-type acoustic metamaterial in an infinite domain.

The sound attenuation of a Helmholtz-type acoustic metamaterial is studied in the quantity of absolute pressure, which is defined as follows

$$|\tilde{p}(r,z,\omega)| = \sqrt{(Re(\tilde{p}(r,z,\omega))^2 + (Im(\tilde{p}(r,z,\omega))^2}. \tag{5.1}$$

5.1.1. Validation of a Single Resonator

Throughout this section, the pressure fields are solved using the BEM with the solution method introduced in chapter 3. To check the validity of the assumptions made in chapter 4, the pressure field containing a single reference resonator is solved using the BEM and the FEM, of which the results are compared. The characteristics of the reference resonator are equivalent to the characteristics obtained in chapter 4 at a depth of 0.5 meter. As listed in Table 5.1, the pressure is measured at a distance of 4 meters from the source, or 2 meters from the centre of the open end of the resonator. The results are plotted in Figure 5.2.

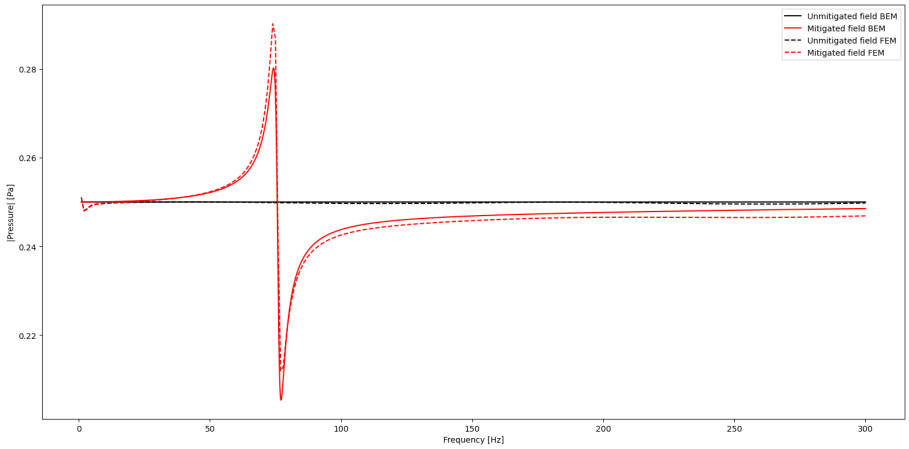

Figure 5.2: Validation of a single resonator in an infinite domain excited by a point source. The mitigated and unmitigated situations, obtained from BEM and FEM, are plotted.

It is observed that the models show qualitative similarities. However, some quantitative differences are observed. Firstly, the pressure response in BEM has a slightly smaller amplification at frequencies below the natural frequency of the resonator and a slightly larger pressure reduction at frequencies above the natural frequency of the resonator. These differences fall within an acceptable range. Additionally, the results of the FEM model show a discrepancy at near-zero frequencies. This is a very minor discrepancy, most probably attributed to the behaviour of the numerical FEM solver at near-zero frequencies, and is therefore negligible.

Because the resonator shows similar behaviour in the BEM and in the FEM, i.e. the shape, location and magnitude of the amplification and the reduction of the pressure field are similar, the lumped-component resonator is considered validated.

5.1.2. Metamaterial with Identical Resonators

In this subsection, a Helmholtz-type acoustic metamaterial with identical resonators is studied. In addition to the characteristics of the resonator, the number of unit cells in the acoustic metamaterial and the distance between them define the configuration of the Helmholtz-type acoustic metamaterial. Therefore, to study the influence of periodicity on the sound pressure attenuation of a Helmholtz-type acoustic metamaterial, a parametric study is conducted, varying the number of unit cells and the distances between them. The arrays consist of N resonators, where N equals 10, 20, 30 or 40. Each array is analysed for five different lattice constants Δr. The results are depicted in Figure 5.3.

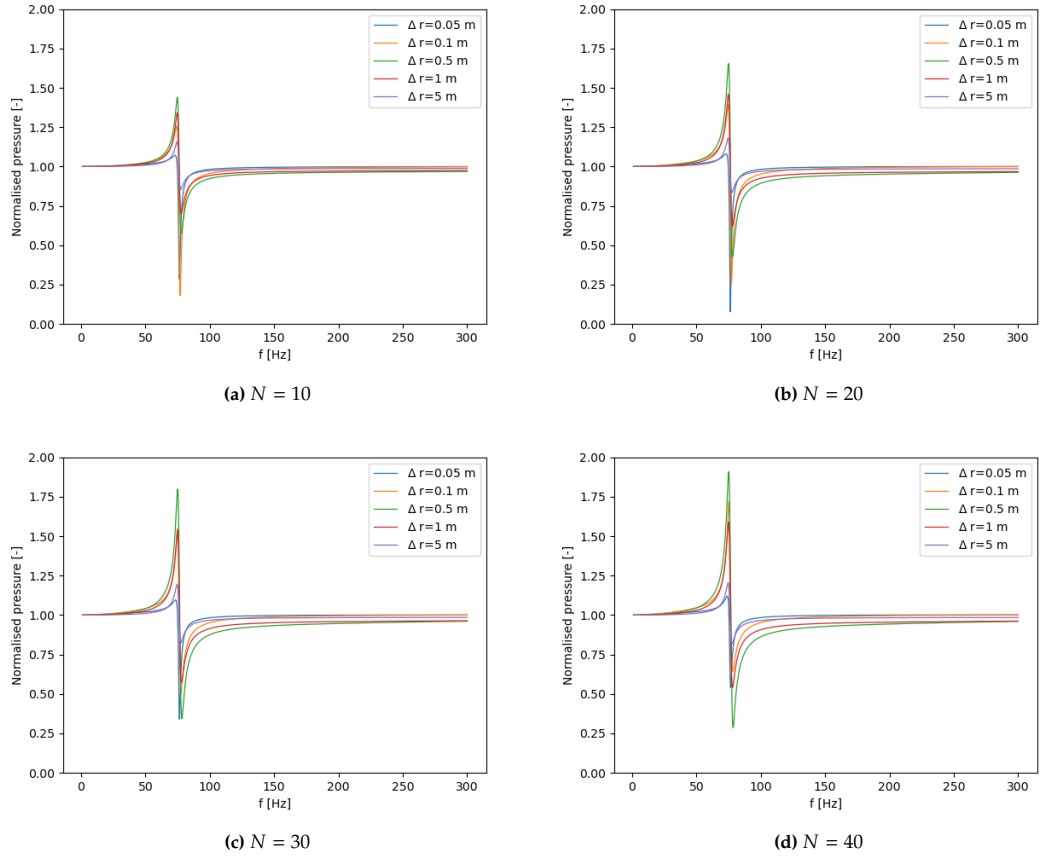

(a) $N = 10$ **(b)** $N = 20$

(c) $N = 30$ **(d)** $N = 40$

Figure 5.3: The absolute pressure in an infinite domain measured at 229 meters from the source, using 20 different configurations of Helmholtz-type acoustic metamaterials with identical unit cells.

According to the theory on phononic crystals, introduced in subsection 2.2.1, a Bragg scattering band gap is expected when the lattice constant of a periodic lattice is a multiple of a half-wavelength of the incident pressure wave. In the results depicted in Figure 5.3, this would be expected at 150 Hz for the system with a lattice constant of 5 meters, for instance. However, no separate Bragg scattering band gap is observed. This is explained by the fact that for a simple point source in an infinite domain, the field is known to propagate as a spherical wave with the medium wave number through an isotropic (uniform speed of sound and directional independence) medium [23]. Additionally, the volumes of the resonators are much smaller than the volume of water of a truncated infinite domain. Therefore, this type of wave propagation does not favour Bragg scattering, which generally relies on directional interference and periodic interactions. From this, the limitations of using a point source in an infinite isotropic medium for studying phenomena like Bragg scattering become clear.

In contrast to the absence of a Bragg scattering band gap, effects related to the lattice constant and number of resonators are clearly observed. Firstly, it is observed that for every increment

of N the amplification of the pressure field at frequencies below the natural frequency of the individual resonators increases. Conversely, the reduction of the pressure field at frequencies above the natural frequency of the individual resonators does not show this consistent behaviour. Interestingly, the configurations with lattice constants of $\Delta r = 0.05$ and $\Delta r = 0.1$ show large reduction of the pressure field at frequencies above the natural frequency of the individual resonators for $N = 10$ and $N = 20$ resonators, whereas this behaviour deteriorates for $N = 30$ and $N = 40$ resonators. The configurations with lattice constants of $\Delta r = 0.5$, $\Delta r = 1$ and $\Delta r = 5$ show constant behaviour, where both the amplification and the reduction of the pressure field increase for each increment of N. Secondly, when comparing the four sub figures in Figure 5.3 it is observed that the magnitude of the pressure is negatively correlated to the number of resonators N for arrays with lattice constants of $\Delta r = 0.5$, $\Delta r = 1$ and $\Delta r = 5$. It shows that the homogenised behaviour decreases for increasing lattice constant, which is in agreement with the first condition on which the principle of a Helmholtz-type locally resonant metamaterial rests (introduced by Liu and Yang (2017) [27], listed in subsection 2.2.2):

If an array of Helmholtz resonators is configured periodically with a lattice constant much smaller than the acoustic wavelength, the periodic system will behave as a homogenised effective medium where a band gap is expected.

For example, consider the configuration with a lattice constant Δr of 5 meters, with a local natural frequency of approximately 75 Hz. In this case the wavelength is approximately 20 meters, which results in the fact that the lattice constant is only a quarter wavelength. Therefore, the condition introduced by Liu and Yang is not valid. This results in a system where the effect of the individual resonators is governing, in stead of the effect of a homogenised behaviour.

Important in these observations is the fact that the unwanted amplification of the pressure at frequencies below the natural frequency of the individual resonators increases dramatically for some configurations, which shows that the system is sensitive for specific combinations of N and Δr. Additionally, it must be noted that the resonators comprising the Helmholtz-type acoustic metamaterials are not mechanically coupled. Therefore, the effects are purely based on acoustic coupling.

5.1.3. Functionally Graded Metamaterial

In the previous section, significant amplification of the pressure field at frequencies below the natural frequency of the individual Helmholtz-type resonators within the arrays is observed. Additionally, the sensitivity of the system is addressed. This section extends the study to examine the effect of functional grading on sound pressure attenuation in a Helmholtz-type acoustic metamaterial within an infinite domain. Functional grading involves configuring metamaterials in a specific manner, leading to different acoustic behaviours compared to their regular counterparts. In this study, functional grading is applied by varying the natural frequencies of the resonators along the length of the array. The influence of this grading on the sound pressure attenuation is then investigated.

An array of $N = 20$ resonators with a lattice constant of $\Delta r = 0.1$ m is placed in an infinite domain. In Figure 5.3b of the previous section, it is observed that this configuration shows a large reduction of the pressure field at frequencies above the natural frequency of the individual resonators, as well as a significant amplification of the pressure field at lower frequencies. Therefore, this configuration is suitable to examine the effects of functional grading on the behaviour of Helmholtz-type acoustic metamaterials. To understand the impact of functional grading, three frequency steps (Δf) are considered: 1 Hz, 2 Hz, and 3 Hz. The natural frequencies are either increased or decreased along the length of the array. In Figure 5.4a, the pressure field results are plotted for a frequency range of 0 Hz to 300 Hz.

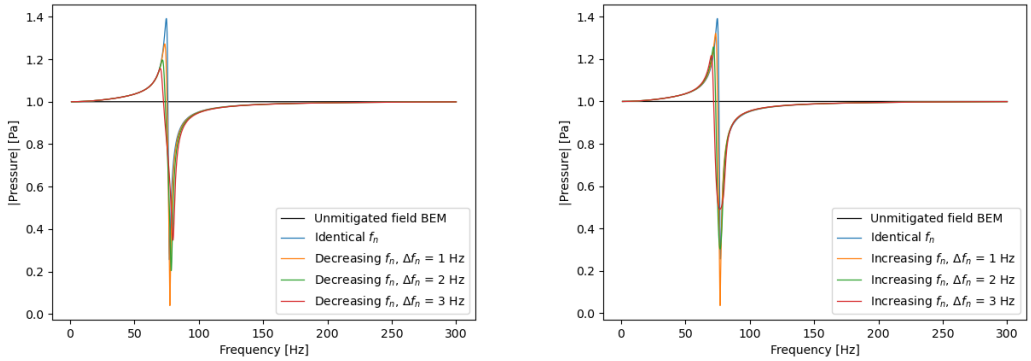

(a) Decreasing natural frequencies

(b) Increasing natural frequencies

Figure 5.4: The absolute pressure in an infinite domain measured at 229 meters from the source, using 6 configurations of functionally graded Helmholtz-type acoustic metamaterials. Figure 5.4a shows functional grading with decreasing increments and Figure 5.4b shows functional grading with increasing increments.

In Figure 5.4, the effects of functional grading on the pressure field are presented. It is observed that for both types of functional grading the amplification of the pressure field is significantly decreased compared to a Helmholtz-type acoustic metamaterial with identical resonators. In some configurations the attenuation increases (1 Hz decreasing, 2 Hz decreasing, 1 Hz increasing), and in some configurations, the attenuation decreases (3 Hz decreasing, 2 Hz increasing, 3 Hz increasing). In accordance with literature on functionally graded metamaterials, functional grading can show improved behaviour.

The reduction in pressure amplification can be explained by considering the resonators with natural frequencies lower than those in the system with identical resonators. These lower frequency resonators shift their influence on the pressure field to lower frequency ranges, thereby reducing the overall amplification in the original frequency range of interest. Interestingly, a functional grading of $\Delta f_n = 1$ Hz shows increased attenuation, whereas this deteriorates for larger Δf_n. This suggests that the homogenised effects, initiated by the locally resonant characteristics, are reduced when the increment (or decrement) in the functional grading becomes too large.

Whilst the reduction of the amplification of the pressure field at low frequencies becomes larger for increasing Δf_n, the noise attenuation decreases. Therefore, the trade-off between these characteristics must be considered. In this thesis, the potential effect of functional grading on the unwanted amplification of the pressure field is investigated. Because of this, functional grading in the form of decreasing natural frequencies with increments of 3 Hz is preferred.

5.2. Vertical System of Helmholtz-type Acoustic Metamaterials

Following the study on identical and functionally graded Helmholtz-type acoustic metamaterials, this section studies a vertical system of multiple Helmholtz-type acoustic metamaterials within a bounded domain and aims to investigate the sound pressure attenuation for different configurations. The setup of the system is depicted in Figure 6.1 and the system parameters are listed in Table 6.1.

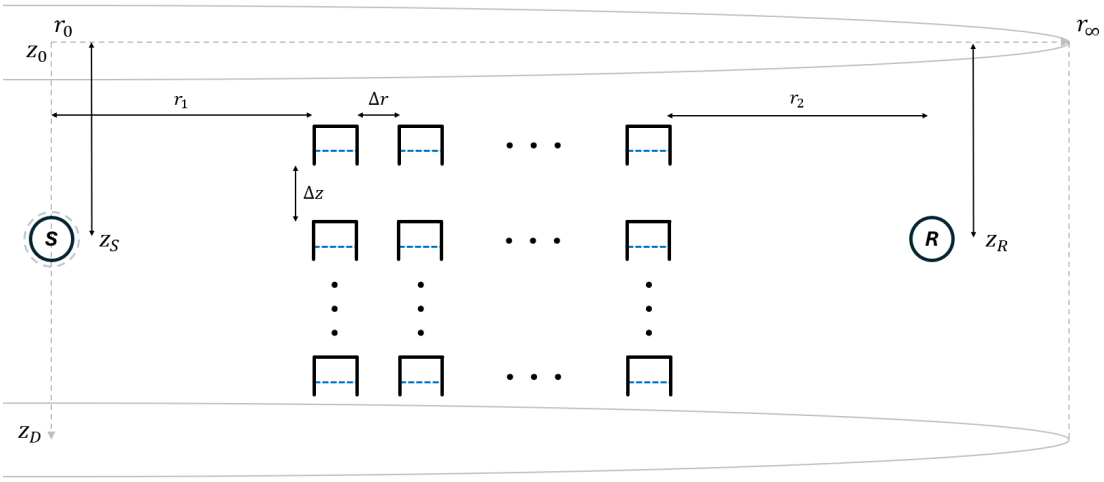

Figure 5.5: Vertical system of Helmholtz-type acoustic metamaterials in a bounded domain excited by a point source. The domain is bound by a pressure release boundary at $z_0 = 0$ m and a rigid boundary at $z_D = 10$ m. A cylindrical radiation condition is considered.

[m]	Validation	Main study
D	1	10
r_1	2	2
r_2	1	1
Δr	-	0.1
z_S	0.5	5
z_R	0.5	5
Δz	-	0.5, 1, 2

Table 5.2: Parameters for a vertical system of Helmholtz-type acoustic metamaterials in a bounded domain.

In contrast to the previous study on Helmholtz-type acoustic metamaterials, which was conducted in absolute pressure, this study is conducted in the quantity of SPL. This is a conventional unit to describe noise reduction in NMSs for offshore impact pile driving and is thus used in this part of the study. SPL is calculated from the absolute pressure as follows:

$$SPL = 10 \log_{10} \left(\frac{\sqrt{2}}{2} \frac{|\tilde{p}_{rms}(r, z, \omega)|^2}{(10^{-6})^2} \right). \tag{5.2}$$

5.2.1. Validation of a Single Resonator

In addition to the validation of a single resonator in an infinite domain, conducted in the previous section, the behaviour of a single resonator must be validated in a bounded domain. The resonator is located in a domain with a depth D of 1 meter, at a water depth z of 0.5 meter and a distance r of 2 meters from the source. The pressure field is solved using both the BEM and the FEM. The results are plotted in the Figure 5.6, where good agreement between the BEM and FEM results is observed. Therefore, the solution method is considered to be validated.

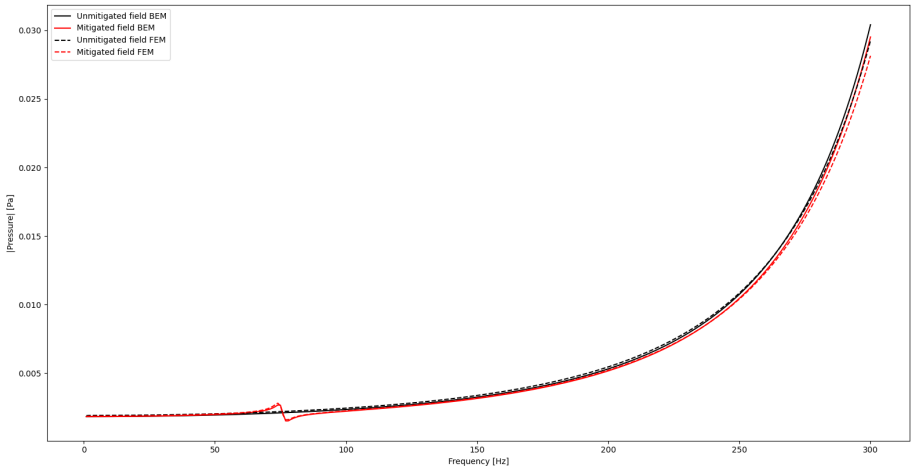

Figure 5.6: Validation of a single resonator in a bounded domain excited by a point source. The mitigated and unmitigated situations, obtained from BEM and FEM, are plotted.

5.2.2. System with Identical Resonators

Helmholtz-resonator based NMSs are convenient near-field systems because the mechanism of trapping air in the cavities of the individual resonators is passive, i.e. the individual resonators fill with air during deployment and the air is naturally compressed because of the hydrostatic pressure. In chapter 4, the natural frequency, spring stiffness and damping ratio are determined for a reference resonator at depths between 0.25 meter and 10 meters. Building on this, this section investigates the acoustic behaviour of a system of Helmholtz-type acoustic metamaterials in different vertical configurations.

The system comprises of horizontal Helmholtz-type acoustic metamaterials with a lattice constant Δr of 0.1 meter. Three vertical configurations are investigated, each with a different vertical spacing Δz. For convenience, the system is discretised into a matrix with M columns and N rows. The number of columns M (i.e. the number of resonators in each horizontal array) is determined on the basis of the previous section and is the same for all three configurations. Each configuration has a different number of rows N (i.e. the number of horizontal arrays). The different combinations are listed in Table 5.3.

Configuration 1	
M = 20	$\Delta r = 0.1$
N = 5	$\Delta z = 2$
Configuration 2	
M = 20	$\Delta r = 0.1$
N = 5	$\Delta z = 1$
Configuration 3	
M = 20	$\Delta r = 0.1$
N = 5	$\Delta z = 0.5$

Table 5.3: Three configurations for a naturally compressed vertical system of Helmholtz-type acoustic metamaterials with identical resonators.

The results of the three studies are plotted in Figure 5.7, where configuration 1 is the blue graph, configuration 2 is the yellow graph and configuration 3 is the green graph. Here, Figure 5.7a shows the response in SPL and Figure 5.7b shows the response in transmission loss (TL), which is obtained by subtracting the mitigated responses from the unmitigated response. It is observed

that for each configuration an amplification of the sound pressure level occurs between 0 Hz and 80 Hz (negative transmission loss), as well as a broad attenuation range between 80 Hz and 180 Hz (positive transmission loss). This observation is in accordance with the results of the previous section where similar amplification and attenuation ranges are distinguished for a single Helmholtz-type acoustic metamaterial. Therefore, it is noted that this is the approximate range of influence of the acoustic metamaterial and is thus attributed to the effects of local resonance. Additionally, it is observed that there are outliers at frequencies of approximately 80 Hz, 110 Hz, 180 Hz and 275 Hz, attributed to the effect of local resonance and the frequencies at which the second, third and fourth normal mode start, respectively. An elaboration on how the normal modes govern the shape of the frequency-domain pressure response of a depth-dependent domain is provided in Appendix B.

The differences between the results of configurations 1, 2, and 3 lie mainly in the magnitudes of the amplification and the attenuation of the sound pressure. An interesting observation is that the attenuation in configuration 2 ($\Delta z = 1$ m) is larger than the attenuation observed in configuration 3 ($\Delta z = 0.5$ m), while it consists of fewer resonators. Therefore, the sound pressure attenuation is sensitive to the vertical distance between the individual Helmholtz-type acoustic metamaterials and the number of resonators of which the system comprises. From this, the configuration consisting of 10 Helmholtz-type acoustic metamaterials with a vertical spacing of $\Delta z = 1$ m, each comprising of $N = 20$ identical resonators with a horizontal spacing of $\Delta r = 0.1$ m, shows the best noise attenuation properties. However, it is noted that the unwanted amplification of the pressure field at low frequencies is the highest for this configuration. In the next section, the effect of functional grading on this unwanted amplification is investigated.

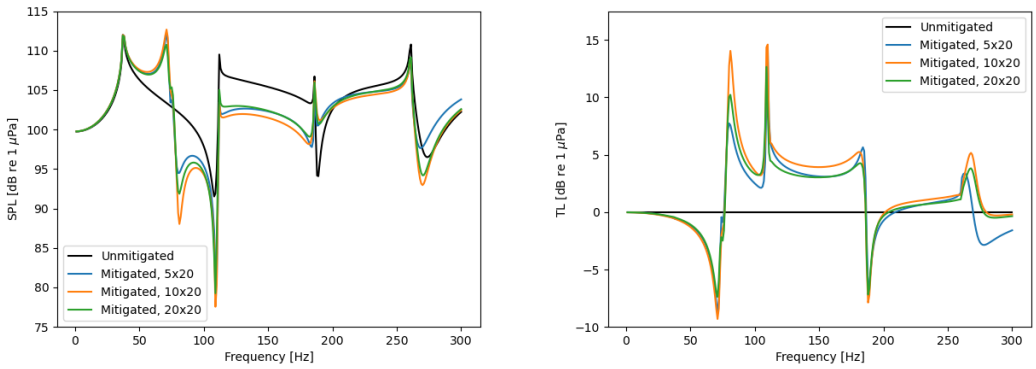

(a) Sound Pressure Level

(b) Transmission Loss

Figure 5.7: Naturally compressed vertical system of Helmholtz-type acoustic metamaterials with identical resonators.

5.2.3. Functionally Graded System

In subsection 5.1.3, it is observed that a functionally graded Helmholtz-type acoustic metamaterial can reduce unwanted amplification of the pressure field for frequencies below the natural frequencies of the individual resonators. Building upon this finding, functional grading is applied to the system studied in the previous subsection, were the unwanted amplification is also observed. The grading is considered in the form of decreasing natural frequencies, with increments of 3 Hz, as this shows the highest reduction of the unwanted amplification of the pressure field with a single Helmholtz-type acoustic metamaterial present (subsection 5.1.3). Three vertical configurations are considered, in which the horizontal spacing of the unit cells and the number of unit cells remain the same. The aim of this subsection is to investigate the effect of functional grading on the transmission loss of a vertical system of Helmholtz-type acoustic metamaterials. In Table 5.4, the additional simulations are listed. The results are plotted in Figure 5.8.

Configuration 1	
M = 20	$\Delta r = 0.1$
N = 5	$\Delta z = 2$
Configuration 2	
M = 20	$\Delta r = 0.1$
N = 10	$\Delta z = 1$
Configuration 3	
M = 20	$\Delta r = 0.1$
N = 20	$\Delta z = 0.5$

Table 5.4: Three studies for a naturally compressed system comprising of functionally graded Helmholtz-type acoustic metamaterials.

Similar to the study of a vertical system of Helmholtz-type acoustic metamaterials with identical resonators in Figure 5.7, the normal-mode outliers are observed at 110 Hz, 180 Hz and 275 Hz. Additionally, a similar broad band of transmission loss is observed between 80 Hz and 180 Hz, as well as negative transmission loss at frequencies below 80 Hz. It is observed that configuration 2 (orange graph) shows the highest transmission loss. Additionally, it is observed that the magnitude of the unwanted amplification is similar for systems with 10 vertical layers and with 20 vertical layers. To clearly show the effect of functional grading, the transmission loss graphs for a vertical system with identical resonators and a functionally graded system are compared in Figure 5.9.

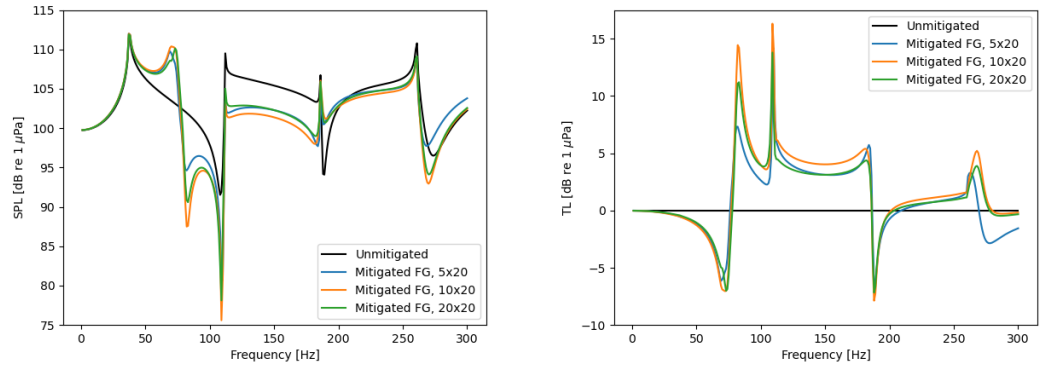

(a) Sound Pressure Level

(b) Transmission Loss

Figure 5.8: Naturally compressed vertical system of Helmholtz-type acoustic metamaterials with functionally graded resonators.

As expected, the effect of functional grading on the system is mainly observed at the local resonance induced sound pressure amplification. The amplification of the sound pressure between 0 Hz and 80 Hz is reduced by approximately 2-3 dB, except for the system with 20 vertical layers. Furthermore, sound pressure attenuation between 80 Hz and 180 Hz increases slightly. These observations are in accordance with the results from subsection 5.1.3.

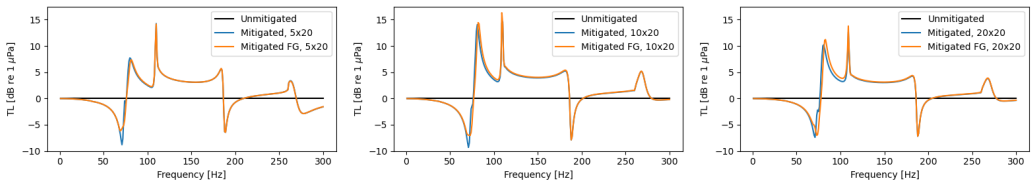

Figure 5.9: One-on-one TL comparison between system with identical resonators and functionally graded system.

5.3. Conclusion

In this chapter, the periodic behaviour of a system of Helmholtz-type resonators is studied. To understand the periodic behaviour of the system, a single horizontal array of Helmholtz-type resonators is first analysed under the excitation of a point source in an infinite domain. Initially, the reference Helmholtz-type resonator is validated by comparing results from the BEM and the FEM. Subsequently, the sensitivity of the lattice constant and the number of resonators in a homogeneous array of Helmholtz-type resonators is studied. Finally, functional grading is applied to the array of Helmholtz-type resonators. These studies provide a comprehensive understanding of the sensitivity of the configuration of a horizontal array of Helmholtz-type resonators.

A functionally graded Helmholtz-type resonator array demonstrates the ability to mitigate the pressure amplification that occurs in a Helmholtz-type acoustic metamaterial with identical resonators. By varying the natural frequencies along the array, the graded configuration redistributes the resonator influence across different frequency ranges, decreasing pressure amplification without reducing attenuation. This behaviour highlights the potential advantages of using functionally graded metamaterials in applications where controlling pressure amplification and maintaining attenuation are important.

Based on the insights obtained from section 5.1, the behaviour of a vertical system of Helmholtz-type acoustic metamaterials under the excitation of a point source in a bounded domain is studied. Again, the reference Helmholtz-type resonator is validated by comparing results from the BEM and the FEM. The depth-dependent lumped-component parameters (ω_m, k, ξ), defined in chapter 4, are applied to each horizontal array of Helmholtz-type resonators. Similar to the study in section 5.1, the vertical system of Helmholtz-type acoustic metamaterials is investigated configuration with identical resonators, and functionally graded configurations.

The results demonstrate that functionally graded vertical systems effectively reduce pressure amplification while maintaining or improving attenuation performance. These findings highlight the potential advantages of functional grading in designing efficient noise mitigation systems for various applications. Additionally, it is found that the noise attenuation of the vertical system of Helmholtz-type acoustic metamaterials is sensitive to the frequency of the source that excited the domain because the noise mitigation occurs in a specific frequency band.

6

Air Volume Reduction in a Vertical System of Helmholtz-type Acoustic Metamaterials

In the introduction to this thesis, the need to develop NMSs tuned to target specific frequency ranges is discussed. It is noted that a Helmholtz-resonator based NMS is a promising solution for reducing underwater noise emitted during offshore impact pile driving, as it is easy to manufacture and highly tunable. However, the performance of the system, in its simplest form, is based on the assumption that the resonators are naturally filled with air during deployment. It is uncertain if the validity of this assumption is continuous throughout the duration of the installation process. Disturbances such as surface waves, currents and the impact pile driving process itself all influence the domain. Moreover, the system returns to its in-air state when retracted. Consequently, it is difficult to monitor whether the air volume in the resonators decreases during the monopile installation process. This chapter investigates the influence of a reduction of encapsulated air on the sound attenuation of a vertical system of Helmholtz-type acoustic metamaterials. The model setup is depicted in Figure 6.1, where the air inside the resonators is highlighted with a blue shading.

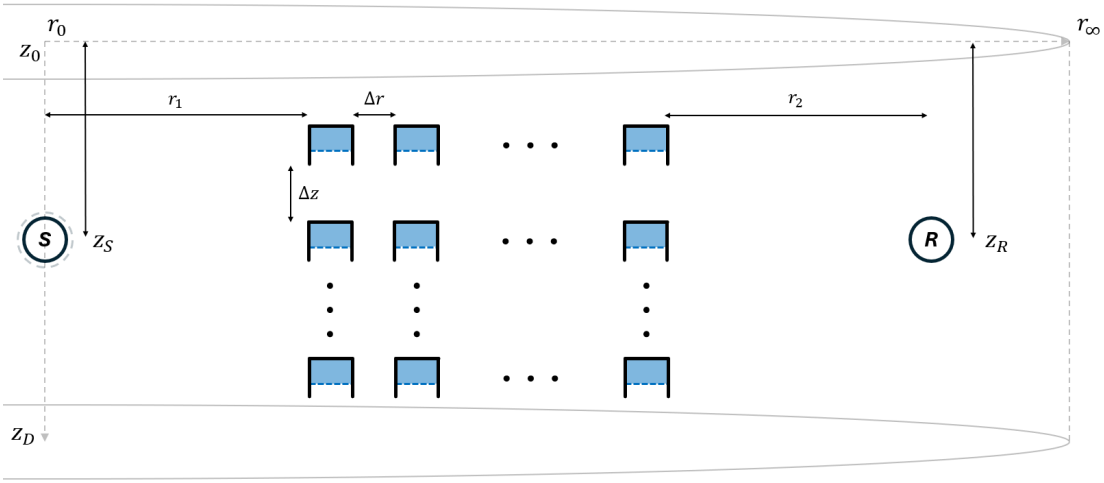

Figure 6.1: Vertical system of Helmholtz-type acoustic metamaterials in a bounded domain excited by a point source. The domain is bound by a pressure release boundary at $z_0 = 0$ m and a rigid boundary at $z_D = 10$ m. A cylindrical radiation condition is considered.

6.1. Frequency-Domain Analysis

In chapter 4, the depth dependent resonator characteristics for a naturally compressed reference resonator are determined. Additionally, the characteristics are determined for reference resonators with a 30% and 70% reduction of encapsulated air. To study the effect of a reduction of encapsulated air on the behaviour of a vertical system of Helmholtz-type acoustic metamaterials, the three sets of resonator characteristics are applied to the system introduced in the beginning of this chapter. The system parameters are listed in Table 6.1. In Figure 6.2, the frequency response functions of the different systems are plotted. Additionally, a transmission loss plot is included.

[m]	Main study
D	10
r_1	2
r_2	1
Δr	0.1
z_S	5
z_R	5
Δz	1
ΔV_a	0%, 30%, 70%

Table 6.1: Parameters for a vertical system of Helmholtz-type acoustic metamaterials in a bounded domain, excited by a point source.

For a decrease in air volume of 30%, it is observed that the frequency range in which sound amplification occurs shifts to slightly higher frequencies. Subsequently, the attenuation range due to local resonance shifts to a slightly higher frequency range, which is in line with the change in natural frequency observed in Figure 4.4a. Furthermore, the unwanted amplification at low frequencies slightly decreases because the spring stiffness slightly increases. The large downward outlier at 110 Hz is exactly at the cut-on frequency of the second propagating mode and is therefore attributed to the semi-analytical solution method. Other than this, in a case where 30% of the air inside the resonators is lost, no extreme sensitivity is observed. However, in a case where the air level inside the resonator decreases by 70% more complex behaviour is observed. The attenuation due to local resonance coincides with the broadband attenuation range between 80 Hz and 180 Hz. Therefore, the positive transmission loss at frequencies above the natural frequencies of the individual resonators is shifted to higher frequencies, which decreases the frequency range in which positive transmission loss occurs (this is observed especially well in Figure 6.2b). Similar to the other graphs, an outlier is observed at the cut-on frequency of the second, third and fourth normal modes. Furthermore, it is observed that the unwanted amplification of the sound pressure level is dramatically decreased. This is in agreement with the steep increase in spring stiffness observed in Figure 4.4b.

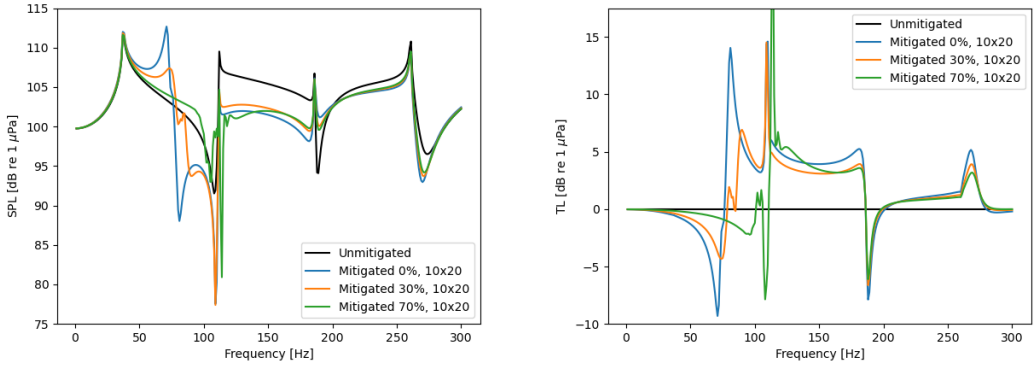

(a) Sound Pressure Level

(b) Transmission Loss

Figure 6.2: Frequency response function of a vertical system of Helmholtz-type acoustic metamaterials, for three different cases (0% air loss, 30% air loss and 70% air loss).

It must be added that the sensitivity (or robustness) of the system is now only analysed on the basis of acoustic coupling. The mechanical coupling, when a Helmholtz-resonator based NMS is fabricated into a mechanical structure, is not taken into account. Therefore, any additional low-frequency resonance, attributed to the structure, is not taken into account.

6.2. Conclusion

This chapter examines how changes in the air volume affect the noise attenuation capabilities of a vertical system of Helmholtz-type acoustic metamaterials. It is found that variations of air volumes in the resonators at a specific water depth impact the lumped component characteristics of the resonator. The natural frequency and the spring stiffness increase if the volume of encapsulated air decreases, whereas the damping ratio decreases. This is in accordance with the theory that describes the lumped component mass-spring-damper.

To investigate the effect of a reduction of encapsulated air on the noise mitigation performance of a Helmholtz-type meta-NMS, systems with a 0%, 30% and 70% reduction of encapsulated air are compared. A 30% reduction of encapsulated air results in a minimal change in the frequency range where sound amplification occurs. Additionally, the frequency range in which positive transmission loss occurs becomes slightly more narrow. These observations are attributed to the fact that the target frequencies are slightly more spread out over depth. However, at this level of reduction, the system still shows behaviour similar to the case without a reduction of air and is therefore robust to a moderate loss of air. At a 70% loss of air, however, the robustness of the system becomes more sensitive. This is expected as the natural frequency, spring stiffness and damping ratio of the resonators all show a significantly larger increment (or decrement) over depth. It is observed that the magnitude of the amplification is decreased dramatically, and that the peak of the amplification is clearly shifted to a higher frequency. This is attributed to the significant increase in natural frequency and spring stiffness of the individual resonators. Because of this, the region of amplification overlaps with the initial frequency range where positive transmission loss occurs, subsequently narrowing the region of transmission loss. This shows that the behaviour of the system is sensitive to a large reduction of encapsulated air, and that this effect is not straightforward to predict. Therefore, the tuning process requires great care. If the amplification of the pressure field shifts to frequencies with higher energy, this can cause dramatic increase in noise. Additionally, if the frequency range in which noise is mitigated becomes more narrow, the noise mitigation properties of the system decrease. Furthermore, any effects because of mechanical coupling expected for an actual Helmholtz-resonator based NMS structure would provide additional low-frequency interaction, which will results in even more unpredictable behaviour. These findings indicate that the performance of the system depends on maintaining an optimal air volume within the resonators.

7

Case Study: Approximation of a Mach Wave from Offshore Impact Pile Driving

In the previous chapters, a single point source is used to investigate the behaviour of different configurations of (systems of) Helmholtz-type acoustic metamaterials. Because of their mathematical simplicity, point sources are a convenient application when researching the behaviour of, and interaction between, acoustically coupled resonators. However, it does not accurately represent the pressure field radiated by a vibrating monopile excited by an impact hammer. To address this limitation, the pressure field radiated by a vibrating monopile is approximated by exciting a vertical array of phased monopole point sources, based on the work of Reinhall and Dahl (2011) [40]. The sources are distributed equally along the z-axis of the domain (Δz_S), at $r_0 = 0$ m. A schematisation of the domain is included in Figure 7.1 and the parameters are listed in Table 7.1

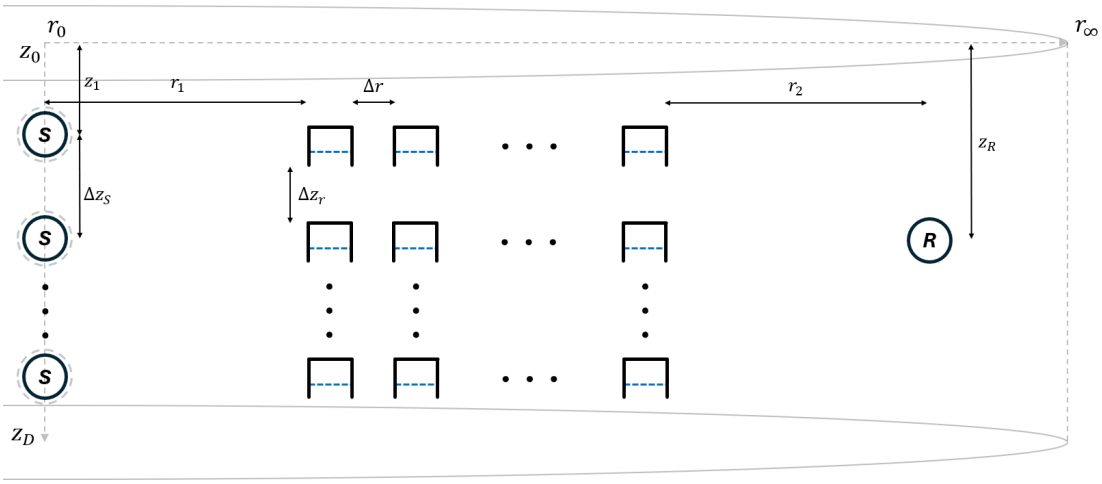

Figure 7.1: Vertical system of Helmholtz-type acoustic metamaterials in a bounded domain excited by an array of 10 phased point sources. The domain is bound by a pressure release boundary at $z_0 = 0$ m and a rigid boundary at $z_D = 10$ m. A cylindrical radiation condition is considered.

Firstly, the definition of the new source term is discussed. Thereafter, the resulting pressure field is analysed. Finally, the noise attenuation of different configurations of a vertical system of Helmholtz-type acoustic metamaterials is investigated.

[m]	Main study
D	10
r_1	2
r_2	2
Δr	0.1
Δz_r	1
Δz_S	1

Table 7.1: Parameters for a vertical system of Helmholtz-type acoustic metamaterials in a bounded domain, excited by an array of phased point sources.

7.1. Acoustic Sources

The most simple representation of an acoustic source is a monopole point source. A monopole point source is a point with negligible geometry (i.e. negligible with respect to its surroundings), that alternately acts as a fluid source and a fluid sink. The frequency, or frequency range, at which this alternation occurs defines the radiated pressure field. For a simple point source, the source term of the inhomogeneous Helmholtz equation is expressed as

$$f(\omega) = S_\omega \delta(\mathbf{r} - \mathbf{r}_0), \tag{7.1}$$

where S_ω represents the amplitude of the source and $\delta(\mathbf{r} - \mathbf{r}_0)$ represents the Dirac delta function. The propagation pattern of a monopole point source is different than that of offshore pile driving noise [17]. In offshore monopile foundation installation, an impact hammer is most widely used to drive the pile into the seabed. The force of an impact hammer can be modelled as a Gaussian-type impulse. However, the response of a hammer impulse is not sufficient to accurately represent the vibrations that are radiated into the water column during pile driving. For instance, Tsouvalas (2014) describes monopiles as high-order, thin-walled shells and the water column (and soil) as a three-dimensional continuous medium [48]. To investigate the behaviour of a vertical system of Helmholtz-type acoustic metamaterials, an approximation of the pressure wave radiated during offshore impact pile driving is sufficient. In chapter 4, chapter 5 and chapter 6 the pressure field is defined by a monopole point source. However, in this chapter the approximation of the pressure field radiated by a vibrating monopile is implemented. Therefore, it is important to briefly elaborate on the influence of the monopile material and shape on the orientation of the pressure wave through the water column.

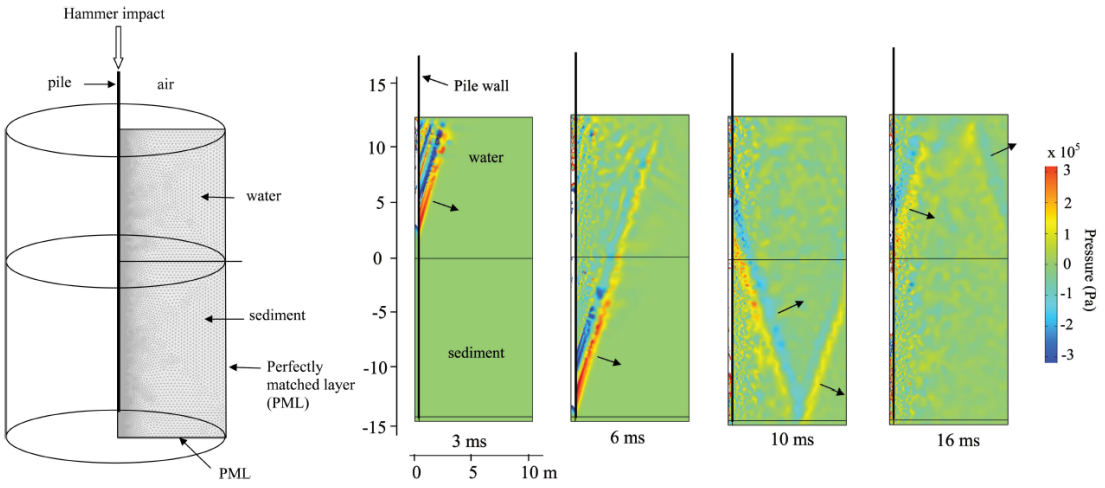

Figure 7.2: Finite element model of a monopile excited by an impact hammer and the resulting pressure field at four different time steps [50][40].

The compressive waves through a monopile due to an impact hammer strike are Mach waves [17]. A Mach wave is a wave of which the speed is greater than its surroundings [40]. Through a

steel solid, the compressive wave travels at a speed of $c_p = 5000$ m/s (at 20 degrees Celsius). The speed of sound through water is $c_w = 1461$ m/s (at 20 degrees Celsius). Therefore, the pressure wave radiates into the water column in a conical pattern. An example of this is provided in Figure 7.2. This conical pattern is called a Mach cone, and its angle is defined by Reinhall and Dahl (2011) [40] as

$$\theta_w = sin^{-1}\left(\frac{c_w}{c_p}\right), \tag{7.2}$$

where θ_w is the angle under which the Mach cone propagates. It is possible to approximate the pressure field resulting from a Mach cone shock wave by using a sequence of point sources with a time delay in the form of a phase lag [37]. In the frequency domain, a point source can be represented by Equation 7.3, where $A(f)$ is the amplitude of the source, f is the frequency and τ is the time delay of the point source, which is equal to the source depth divided by the speed of sound through the monopile.

$$S_\omega = A(f)e^{i2\pi f\tau}. \tag{7.3}$$

To approximate a vibrating monopile, the source strength $A(f)$ is defined by an amplitude weighting spectrum, which Reinhall and Dahl (2011) derived from measurements (Figure 7.3). For the sake of simplicity, this research does not implement a weighted amplitude spectrum. Instead, a uniform amplitude is assumed.

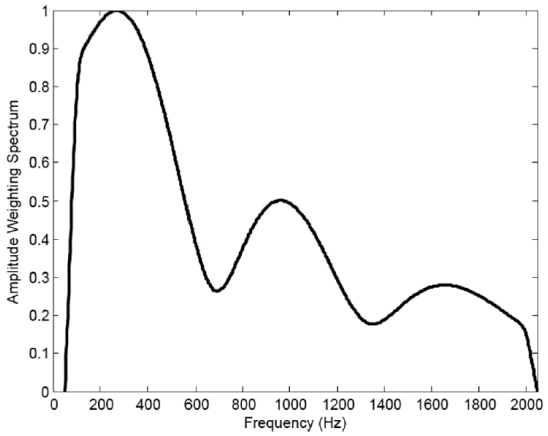

Figure 7.3: Amplitude weighting spectrum [40].

7.2. Unmitigated Pressure Field in Frequency Domain

On the basis of the method for creating a monopile-like source in the form of an array of monopole point sources introduced in section 7.1, this section discusses the pressure field resulting from such a source type. The pressure field is plotted along a 2D slice for individual source frequencies of $f = 75$ Hz (Figure 7.4a) and $f = 300$ Hz (Figure 7.4b). In total, 10 monopole point sources are included in a bounded domain in FEM, as introduced in section 3.3. Similar to the point sources in the frequency-domain simulations conducted in the previous chapters, the individual point sources have an amplitude of 1 N/m.

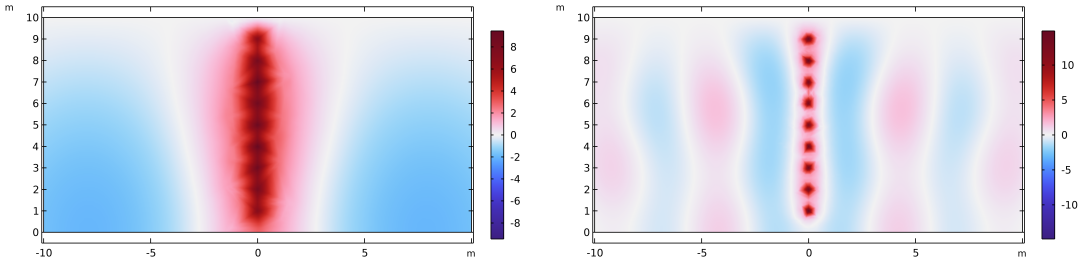

(a) 75 Hz. **(b)** 300 Hz.

Figure 7.4: Pressure field of a schematised monopile source, consisting of 10 phased point sources.

It is important to note that a frequency-domain representation of a pressure field induced by an array of phased point sources does not capture transient shock wave formation. Therefore, a Mach cone pressure wave can not be observed. However, the spatial structure of a Mach cone pressure wave can be observed by analysing the amplitudes and the phase changes of the pressure field in frequency domain. In Figure 7.4, it is observed that the line along which the pressure is equal to zero (zero-pressure line, caused by destructive interference) is predominantly straight for a source frequency of 75 Hz, whereas the the zero-pressure lines show a more complex pattern at 300 Hz. This is explained by the fact that the phase change is proportional to the frequency of the source. From Figure 7.4a, the geometry and angle of the Mach cone can be deduced, which are in accordance with the expected shape of the actual Mach cone pressure wave introduced by Reinhall and Dahl (2011) [40]. Additionally, Figure 7.4b shows finer details of the interaction between different wavefronts at 300 Hz, which is a result of more rapid phase changes. The corresponding phase plots are included in Appendix F.

As the pressure wave propagates under an angle, it is hypothesised that a vertical orientation is not optimal for an underwater Helmholtz-type resonator. Considering the assumption that the pressure is equal over the entire surface of the open end of the resonator, the mass of the resonator (water inside the resonator) can only move vertically. Therefore, it is expected that the resonator is excited optimally if the pressure wave propagates in the direction of the degree of freedom of the resonator. This hypothesis is tested in the next section.

7.3. Transient Response of a Mitigated Pressure Field

To investigate the relationship between the orientation of the resonators in a system of Helmholtz-type acoustic metamaterials and the angle under which the pressure wave propagates, four frequency-domain simulations are conducted using the FEM. Firstly, the pressure field is produced without resonators present. Thereafter, three mitigated pressure fields are produced. The resonators within the Helmholtz-type meta-NMS are positioned under three different angles in the rz-plane: -34 degrees, 0 degrees and 17 degrees. The domain is excited by the array of monopole point sources introduced in the previous section. The pressure is measured at $r = z = 5$ m, after which the inverse Fourier transform is applied to obtain the time-domain response (Appendix E). The results are plotted in Figure 7.5. Two main observations are discussed below.

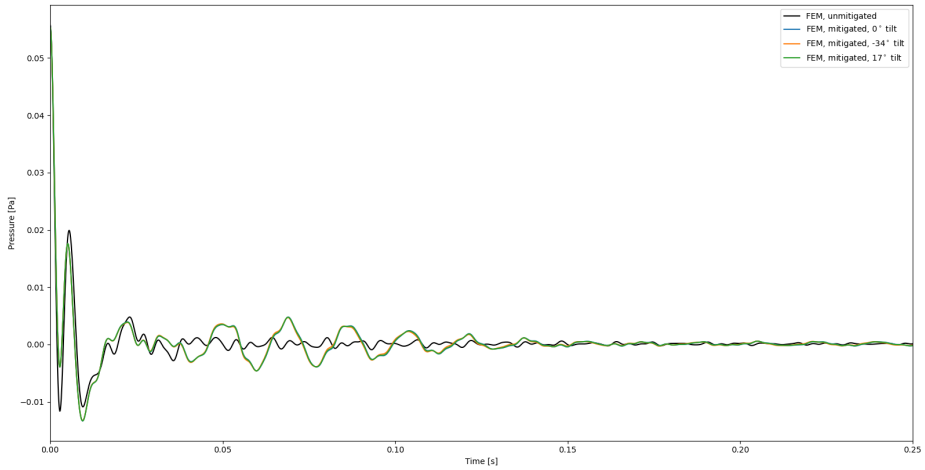

Figure 7.5: Transient pressure response at $r = 5$ m and $z = 5$ m for three vertical systems of Helmholtz-type acoustic metamaterials with different resonator orientations.

Firstly, it is observed that the orientation of the resonators within the system of Helmholtz-type acoustic metamaterials does not significantly influence the pressure response. From this study, it is not clear why no distinct differences are observed. Therefore, additional analysis is required. At the end of this section, the SEL of the different configurations is analysed.

Secondly, it is observed that the pressure response is amplified after approximately 0.04 seconds, in the domains with resonators present. In order to further analyse the signals and substantiate this observation, a time-frequency analysis is conducted. A time-frequency analysis is an analysis that simultaneously studies time and frequency domains. The time signal is sectioned into bins, where each bin represents a unique part of the time signal. Each bin shows the amplitude of the frequency, or frequencies, of which that section of the impulse is built up. In Figure 7.6, time-frequency plots of two of the signals from Figure 7.5 are depicted; the unmitigated signal and the signal mitigated by the system of vertically orientated resonators.

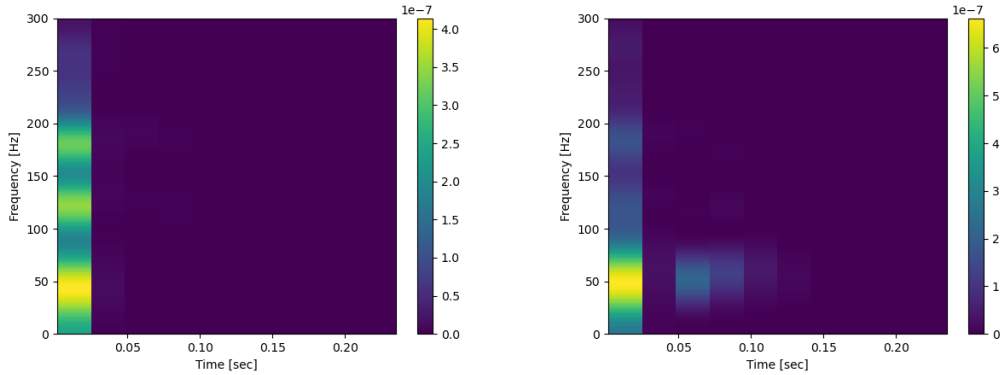

(a) Unmitigated.

(b) Mitigated.

Figure 7.6: Time-frequency analysis.

In Figure 7.6a, it is observed that the governing frequency of the first bin, which corresponds to the first 0.025 seconds of the signal, is in the range of 40-50 Hz, with additional frequencies centred around 125 Hz and 175 Hz. In Figure 7.6b, it is observed that the magnitude of the energy at the two high frequencies reduces and that the governing frequency of the mitigated

signal is concentrated around 50 Hz. This suggests that, in the first 0.025 seconds of the impulse, the energy is transferred from high to low frequencies when resonators are present, which is in accordance with the frequency-domain results obtained in chapter 5. A drawback of analysing the entire transient response is that the details in the part of the signal with low amplitudes (i.e. after the first bin) get lost in the time-frequency plot because the scale is based on the highest amplitude of the signal, which is present in the first 0.025 seconds of the impulse. Therefore, a snippet of the signal is produced to analyse the rest of the transient response.

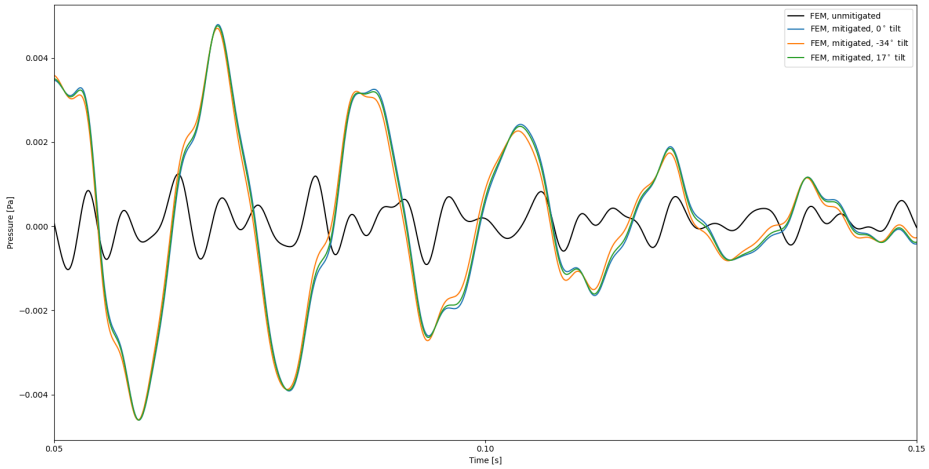

Figure 7.7: Snippet of the time series introduced in Figure 7.5.

In the figure above, a snippet (0.05 to 0.15 seconds) of the original signals plotted in Figure 7.5 is depicted. It is observed that, because the scale of the y-axis is smaller, this section of the signal shows more details than the corresponding section in Figure 7.5. This is confirmed by the time-frequency plots of the snippet, included in the figure below. It is important to note that the scaling between the two time-frequency plots is still different, which is in accordance with the amplitudes of the pressure response in Figure 7.7. Nonetheless, Figure 7.8 shows a clear breakdown of the governing frequencies within the signals.

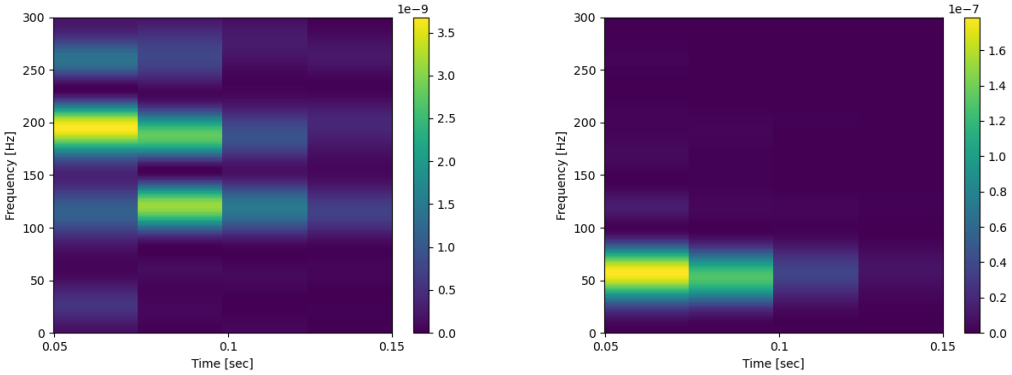

(a) Unmitigated.

(b) Mitigated.

Figure 7.8: Time-frequency analysis.

It is observed that the governing frequencies in this section of the unmitigated signal are much higher than 50 Hz, whereas in the mitigated signal they are concentrated between 50 Hz and 75

Hz. From chapter 5, it is known that for a Helmholtz-type meta-NMS with identical resonators amplification occurs at frequencies between 0 and 75 Hz, with the highest amplifications between 50 Hz and 75 Hz. When combining the observations made when analysing the time-frequency plots in Figure 7.6 and Figure 7.8, it is found that the presence of the resonators amplifies the low-frequency contribution of the transient response and reduces the high frequency contribution of the response. This is again in accordance with the frequency-domain results obtained in chapter 5.

To investigate the influence of the manipulation of different parts of the transient response discussed above, the transient responses are analysed by calculating the single event time-integrated sound pressure level, usually called the sound exposure level (L_E). This provides the sound pressure level of an isolated single sound impulse, or transient sound, over a stated time interval T. The sound exposure level is defined as

$$L_E = 10log_{10}\left(\frac{\int_{t_1}^{t_2} p^2(t)dt}{E_0}\right), \tag{7.4}$$

where $p(t)$ is the pressure at time t, t_1 and t_2 denote the beginning and the end of the impulse time interval T and E_0 is the reference pressure value ($10^{-6}\ Pa^2s$ in water). The results are included in Table 7.2.

Configuration	SEL [dB]
Unmitigated	69.29
0° tilt	69.77
-34° tilt	69.73
17° tilt	69.75

Table 7.2: Sound exposure level of the four transient pressure responses plotted in Figure 7.5.

Interestingly, the sound exposure levels are very similar for all four configurations. Firstly, the results suggest that the system of Helmholtz-type acoustic metamaterials does not actually mitigate the transient sound. It is important to note, however, that the sources used to obtain the transient responses are impulses with identical amplitudes for each frequency. It is known that the pressure waves radiated by a vibrating monopile can be defined by a weighted amplitude spectrum. An example of such an amplitude weighting spectrum is defined by Reinhall and Dahl (2011) and depicted in Figure 7.3, where the highest amplitudes are present at frequencies between 100 Hz and 400 Hz [40]. From this, it is deduced that there is much more energy present in the frequency range where transmission loss would occur, compared to the frequency range that would be amplified. Therefore, these observations must be taken with great care. Secondly, it is observed that the L_E measurements in the domains in which tilted resonators are included show a very minimal decrease in L_E measurement compared to the domain in which vertically orientated resonators are included. In addition to this, it must be noted that the tilt of a resonator changes the shape of the air- and water volume inside the resonator. A result from this is that the encapsulated air inside the resonator becomes more prone to leakage during operation, causing uncertain behaviour of the system (discussed in chapter 6). This, in combination with the minimal magnitude of the difference in SEL, suggests that a vertically orientated resonator is most effective.

7.4. Conclusion

In this chapter, the pressure field resulting from a phased array of monopole point sources is produced, approximating the pressure field corresponding to a vibrating monopile excited by an impact hammer. It is noted that the geometry and angle of the Mach cone are in accordance with the expected shape of a Mach cone pressure wave approximating a pressure wave radiated by a vibrating monopile. From this, it is hypothesised that the orientation of a Helmholtz-type resonator influences its performance. This hypothesis is tested by introducing a vertical system of

Helmholtz-type acoustic metamaterials with tilted resonators into the domain and examining the corresponding transient responses. Analysis of the transient responses shows that the orientation of the resonator does not significantly influence the transient response of the Helmholtz-type meta-NMS. Additional reasoning suggests that a vertical orientation is most feasible, as this respects the geometrical simplicity and robustness of an open-ended resonator most.

Furthermore, the behaviour of the transient responses for a mitigated and an unmitigated system are analysed. It is observed that the impulse is initially mitigated. However, the frequency of the mitigated transient response becomes lower, and the amplitude increases. This is in accordance with the results obtained in chapter 5, where it is observed that the low-frequency component of the response is amplified and the high-frequency component of the response is mitigated. Therefore, the governing frequency of the mitigated transient response is concentrated at 50-75 Hz. An important consideration regarding this observation is that the amplitude spectrum of the source is unweighted, or constant, whereas the amplitude spectrum of a realistic vibrating monopile is weighted. Therefore, it is expected that the mitigation of the transient response using a weighted amplitude spectrum increases. From this, it is concluded that the performance of the system is sensitive to type of source, especially its frequency spectrum, and should therefore always be carefully tuned to its target frequency.

8

Conclusions and Recommendations

This thesis aims to contribute to the knowledge base of periodic, low-frequency NMSs for offshore impact pile driving through literature research, semi-analytical modelling and numerical modelling. In this chapter, the research questions are answered based on the sub conclusions drawn throughout this research. Additionally, the limitations discussed in the introduction to this thesis are recalled, and their implications are discussed. Finally, recommendations for future work are provided.

8.1. Conclusions

The main research question of this thesis reads: *What is the optimal configuration of a periodic Helmholtz-type NMS for offshore impact pile driving* To answer this research question, the following studies have been conducted. Firstly, the behaviour of a single, horizontal array of Helmholtz-type resonators is studied in multiple configurations. The key findings are:

1. Local resonance causes amplification of the pressure field at frequencies below the natural frequency of the individual resonators within the array.
2. Local resonance causes reduction of the pressure field at frequencies above the natural frequency of the individual resonators within the array.
3. The effects of local resonance are more pronounced for arrays with a smaller lattice constant.
4. The effects of local resonance are more pronounced for arrays with a larger number of resonators.
5. Functional grading demonstrates the ability to reduce this amplification, while maintaining the reduction of the pressure field.

Secondly, the behaviour of a Helmholtz-type NMS comprising of multiple horizontal arrays of Helmholtz-type resonators with depth-dependent characteristics, evenly spaced throughout the water column, is studied in multiple configurations. The key findings are:

1. Similar to the results of the study above, the amplification and reduction of the pressure field due to local resonance is observed.
2. The amplification and reduction of the pressure field is larger if more horizontal arrays of resonators are included in the domain (i.e. the vertical gap between each layer decreases).

Thirdly, a case study examining the effect of a Helmholtz-type NMS on an approximation of a pressure field radiated by a vibrating monopile. Here, a vertical array of point sources, activated with a phase lag, produces a pressure field which is examined in the time domain. The key findings are:

1. The local orientation of the individual resonators does not significantly influence the noise mitigation performance of a Helmholtz-type NMS.
2. The low-frequency component of the transient response is amplified, whereas the high-frequency component of the transient response is mitigated. In other words, energy is transferred from high to low frequencies.
3. In the case of an array of sources with an unweighted amplitude spectrum, the sound exposure level is not reduced when a system of Helmholtz-type acoustic metamaterials is implemented. However, it is expected that the sound exposure level will be reduced when a realistic, weighted amplitude spectrum is applied.

On the basis of these results, the main research question is answered as follows:

A Noise amplification is expected at frequencies below the natural frequency of the individual Helmholtz-type resonators within the system, and noise attenuation is realised at frequencies above the natural frequency of the individual Helmholtz-type resonators within the system. Therefore, the energy in high frequencies is transported to low frequencies. Horizontal arrays of 20 resonators with a horizontal spacing of 0.1 meter, and a vertical spacing of 1 meter between each array show a promising balance between the magnitude of the attenuation and the unwanted amplification.

B Functional grading, in the form of incrementally decreasing the natural frequencies of the individual resonators in steps of up to 3 Hz along each horizontal array, demonstrates the ability to reduce this pressure amplification while also providing improved noise attenuation. This is therefore a promising addition to the configuration of a Helmholtz-type NMS.

C A vertical resonator orientation is most feasible, respecting the simplicity and robustness of the open-ended resonator.

In addition to the main research question, two research sub-questions are drafted. The first research sub-question reads: *How does the air-water ratio of the resonators inside a Helmholtz-type NMS influence its noise reduction properties?* To answer this question, the depth-dependent characteristics are determined for two additional situations: a 30% reduction of air volume inside the resonators and a 70% reduction of air volume inside the resonators. The key findings are:

1. In the case of a 30% reduction, the amplification of the pressure field is reduced. However, the noise mitigation is slightly reduced as well.
2. A reduction of 70% of the air inside the resonators reduced the unwanted amplification dramatically. However, it causes noise mitigation to occur at a frequency of 50 Hz more than the benchmark case (0% air reduction).

From this, it is concluded that the system is sensitive to a large reduction of air volume inside the resonators.

The second research sub-question reads: *How does the tilt of the resonators inside a Helmholtz-type NMS influence its noise reduction properties?* This question is answered by examining the transient response of a vertical, phased array of point sources mimicking a vibrating monopile in FEM, and comparing three cases where resonators are included under different orientations. The key finding is:

1. The noise attenuation does not significantly increase if the resonators are tilted, compared to vertically orientated resonators.

From this, it is concluded that the Helmholtz-NMS attenuates noise most efficiently if the resonators are orientated vertically.

This study demonstrates the effect of periodicity in a Helmholtz-type NMS for offshore impact pile driving. An important take-away, based on the conclusions above is that the system can be sensitive to the type of force, especially the frequency at which the force radiates pressure waves. For instance, it is known that the bulk of the energy radiated by a monopile during pile driving

is in the lower end of the frequency spectrum. Especially if air is lost from the system during the pile driving process, the risk of amplifying the pressure field increases.

8.2. Limitations

In the introduction (chapter 1), the limitations of this thesis are briefly introduced by defining the scope of the study. Based on this, the implications of these limitations are discussed in this section:

- **Source.** In the bulk of this thesis, a point source is used to radiate a pressure wave into a domain. It is clear that the pressure wave radiated by a point source does not accurately represent the pressure wave radiated by a vibrating monopile. In order to accurately model noise from offshore impact pile driving, an array of phased point sources is not sufficient either. One of the main consequences of this is that the source amplitude spectrum is not accurately described. If the results are misinterpreted, or if the limitations are not carefully considered, this can in potentially misleading conclusions. For instance, the sound exposure level calculations in chapter 7 show that the system does not actually mitigate the single event time-integrated sound pressure level. However, the results do clearly show the frequency-dependency of the Helmholtz-type meta-NMS. Therefore, it is concluded these results are strongly related to the assumption that the amplitude spectrum is constant, instead of weighted.

- **Seabed.** The seabed is modelled as a rigid, fully reflective boundary in the studies considering a bounded domain. In reality, pressure waves that are radiated into the soil through the monopile are also re-radiate into the water column. In order to properly include the influence of the soil into the model, sophisticated acoustic wave propagation models, lab testing and field testing is required. However, as a near field NMS is not designed to mitigate pressure waves that are radiated into the water column from the soil, this limitations is not governing in the study of the acoustic coupling of the resonators within a Helmholtz-resonator based NMS. Nonetheless, it must be noted that in reality additional, soil-related, pressure dynamics are expected in the far field.

- **Damping.** The damping ratio has been determined by applying ideal gas theory to the pressure at the open end of a resonator obtained from COMSOL Multiphysics. Contradictory, COMSOL Multiphysics requires user-defined damping as a model input. Therefore, the user-defined damping governs the resulting damping ratio. As discussed in chapter 4, damping is included in COMSOL Multiphysics in the form of a complex speed of sound. In order to properly define the damping of a Helmholtz-type resonator, the attenuation characteristics must therefore be correctly defined first. For instance, reflection and scattering at the shell of the resonators must be examined, as well as visco-thermal losses within the resonator cavity.

- **Mechanical Coupling.** In this study, the acoustic coupling between individual Helmholtz-type resonators in a system of Helmholtz-type resonators is studied. When considering an actual Helmholtz-resonator based NMS, the resonators are embedded within a structure. Therefore, it is expected that the response of the actual system and its mechanical coupling will be different. This will, most likely, influence the low-frequency spectrum of the response. It is important to note that amplification of the pressure field is expected at low frequencies. Therefore, the behaviour at low-frequencies will be even more sensitive when the actual structure is modelled.

- **Offshore Conditions.** This study is conducted in a controlled virtual environment. In other words, the potential influence of the current, surface waves and vessel interaction is not considered. It must be noted that the performance of the system is very much dependent on the volume of encapsulated air within the individual Helmholtz-type resonators. Therefore, the conclusions drawn in this study are always with careful consideration of the approximations and simplifications.

8.3. Recommendations

On the basis of the limitations discussed in the previous section, recommendations for future research are discussed. As mentioned in the previous section, there are uncertainties regarding the damping characteristic of a Helmholtz-type resonator. In a conventional Helmholtz resonator, attenuation occurs in the form of visco-thermal losses in the neck and cavity. Additionally, in many applications refraction, reflection and scattering also occur. However, in an offshore application much is unknown about the attenuation of a Helmholtz-type resonator. Therefore, it is interesting to conduct a series of controlled physical scale tests in which the damping characteristics of a Helmholtz-type resonator, or an array of Helmholtz-type resonators, is investigated.

In addition to the acoustic interaction between individual Helmholtz-type resonator and its influence on the noise mitigation of an Helmholtz-resonator based NMS, it is mentioned that the dynamics of the structure of the NMS will have an influence on its noise mitigation performance. From literature, it is known that the collective resonance of the NMS structure acts in the low-frequency end of the noise spectrum. To predict the behaviour of a Helmholtz-resonator based NMS with fewer uncertainties, a full structure including a frame and the arrays of Helmholtz-type acoustic metamaterials must be modelled. This can be done, for instance, by mechanically coupling the individual resonators through a series of springs or rods with characteristics similar to that of a steel frame. By comparing this to a system where the Helmholtz-type resonators are modelled individually, without mechanical coupling, a better understanding of the acoustic behaviour of the full system is obtained. It is expected that the sound pressure is amplified at very low frequencies. For monopiles with a relatively small diameter (compared to XXL monopiles), this does not pose a big problem as the energy in the pressure wave radiated during offshore impact pile driving is lower at low frequencies. However, it is expected that for larger monopiles (diameter of 11 meters) low frequencies become more governing. Therefore, the structural resonance of a near-pile NMS can amplify the governing frequencies, causing a dramatic increase in sound pressure level. In addition to this, it is possible that the frequency range at which this amplification becomes broader if the volume of encapsulated air in the resonators decreases during operation, or if the system is not tuned to the correct monopile or environment. In this case, the low-frequency behaviour of the system becomes even more unpredictable.

Based on the above, an interesting new field of research lies in the composition of the structure of near-pile NMSs. For instance, metamaterial theory can be used to design a structure that is capable of mitigating structural vibrations in specific frequency ranges through stop bands, in addition to the stop bands obtained from the acoustic coupling of the resonators within the structure. In this case, additional frequency ranges can be targeted, or the low-frequency excitation of the structure can be reduced.

References

[1] AdBm Technologies. 2020. URL: https://adbmtech.com/.

[2] M Alster. "Improved calculation of resonant frequencies of Helmholtz resonators". In: *Journal of sound and vibration* 24.1 (1972), pp. 63–85.

[3] Helen Bailey et al. "Assessing underwater noise levels during pile-driving at an offshore windfarm and its potential effects on marine mammals". In: *Marine pollution bulletin* 60.6 (2010), pp. 888–897.

[4] Yue Bao et al. "Design of Helmholtz resonator group in a lightweight aluminum alloy wheel for reducing tire acoustic cavity resonance noise". In: *Applied Acoustics* 201 (2022), p. 109124.

[5] Michael A Bellmann et al. "Is there a state-of-the-art to reduce pile-driving noise?" In: *Wind Energy and Wildlife Interactions: Presentations from the CWW2015 Conference*. Springer. 2017, pp. 161–172.

[6] Valter Bellucci et al. "On the use of Helmholtz resonators for damping acoustic pulsations in industrial gas turbines". In: *J. Eng. Gas Turbines Power* 126.2 (2004), pp. 271–275.

[7] CE Bradley. "Time harmonic acoustic Bloch wave propagation in periodic waveguides. Part I. Theory". In: *The Journal of the Acoustical Society of America* 96.3 (1994), pp. 1844–1853.

[8] Leon Brillouin. "Wave propagation in periodic structures". In: (1946).

[9] CAI Chenzhi and Cheuk Ming Mak. "Noise attenuation capacity of a Helmholtz resonator". In: *Advances in Engineering Software* 116 (2018), pp. 60–66.

[10] Michael Dähne et al. "Bubble curtains attenuate noise from offshore wind farm construction and reduce temporary habitat loss for harbour porpoises". In: *Marine Ecology Progress Series* 580 (2017), pp. 221–237.

[11] JO Daniel. "Automotive wheel and tyre design for suppression of acoustic cavity noise through the incorporation of passive resonators". In: *Journal of Sound and Vibration* 467 (2020), p. 115037.

[12] JA David. "Likely sensitivity of bottlenose dolphins to pile-driving noise". In: *Water and Environment Journal* 20.1 (2006), pp. 48–54.

[13] Vladimir Fokin et al. "Method for retrieving effective properties of locally resonant acoustic metamaterials". In: *Physical review B* 76.14 (2007), p. 144302.

[14] SiF Offshore Foundations. Hollandse Kust Zuid. (2024). URL: https://sif-group.com/nl/producten-en-services/referenties/hollandse-kust-zuid/.

[15] SiF Offshore Foundations. Monopiles and Transition Pieces. (2024). URL: https://sif-group.com/en/monopiles-and-transition-pieces/#monopiles.

[16] Frank Gerdes et al. "Measurements of pile driving noise at the research platform FINO3". In: *INTER-NOISE and NOISE-CON Congress and Conference Proceedings*. Vol. 253. 6. Institute of Noise Control Engineering. 2016, pp. 2844–2851.

[17] Dong-Gyun Han and Jee Woong Choi. "Measurements and spatial distribution simulation of impact pile driving underwater noise generated during the construction of offshore wind power plant off the southwest coast of Korea". In: *Frontiers in Marine Science* 8 (2022), p. 654991.

[18] H von Helmholtz. "Theorie der Luftschwingungen in Röhren mit offenen Enden." In: (1860).

[19] Hermann von Helmholtz. *On the Sensations of Tone as a Physiological Basis for the Theory of Music*. Longmans, Green, and Co., 1885.

[20] James E Herbert-Read et al. “Anthropogenic noise pollution from pile-driving disrupts the structure and dynamics of fish shoals”. In: *Proceedings of the Royal Society B: Biological Sciences* 284.1863 (2017), p. 20171627.

[21] MS Howe. “On the Helmholtz resonator”. In: *Journal of Sound and Vibration* 45.3 (1976), pp. 427–440.

[22] Mahmoud I Hussein, Michael J Leamy, and Massimo Ruzzene. “Dynamics of phononic materials and structures: Historical origins, recent progress, and future outlook”. In: *Applied Mechanics Reviews* 66.4 (2014), p. 040802.

[23] Finn B Jensen et al. *Computational ocean acoustics*. Vol. 2011. Springer, 2011.

[24] John D Joannopoulos, Pierre R Villeneuve, and Shanhui Fan. “Photonic crystals”. In: *Solid State Communications* 102.2-3 (1997), pp. 165–173.

[25] MC Junger. “Helmholtz resonators in load-bearing walls”. In: *Noise Control Engineering* 4.1 (1975), pp. 17–25.

[26] Stephan Lippert et al. “COMPILE—A generic benchmark case for predictions of marine pile-driving noise”. In: *IEEE Journal of Oceanic Engineering* 41.4 (2016), pp. 1061–1071.

[27] Boyun Liu and Liang Yang. “Transmission of low-frequency acoustic waves in seawater piping systems with periodical and adjustable helmholtz resonator”. In: *Journal of Marine Science and Engineering* 5.4 (2017), p. 56.

[28] Guancong Ma and Ping Sheng. “Acoustic metamaterials: From local resonances to broad horizons”. In: *Science advances* 2.2 (2016), e1501595.

[29] Federal Maritime and Hydrographic Agency. Noise Mitigation Screen (IHC-NMS). URL: https://www.bsh.de/EN/TOPICS/Offshore/Environmental_assessments/Underwater_sound/_Module/Karussell/_documents/Artikel_IHC-System.html.

[30] Federal Maritime and Hydrographic Agency. Hydro Sound Damper (HSD). URL: https://www.bsh.de/EN/TOPICS/Offshore/Environmental_assessments/Underwater_sound/_Module/Karussell/_documents/Artikel_Hydro-Sound-Damper.html.

[31] Christina Mueller-Blenkle et al. “Effects of pile-driving noise on the behaviour of marine fish”. In: (2010).

[32] COMSOL Multiphysics. Perfectly matches Layers (PMLs). URL: https://doc.comsol.com/5.5/doc/com.comsol.help.aco/aco_ug_pressure.05.106.html.

[33] Georg Nehls et al. “Noise mitigation during pile driving efficiently reduces disturbance of marine mammals”. In: *The effects of noise on aquatic life II*. Springer. 2016, pp. 755–762.

[34] Rijksdienst voor Ondernemend Nederland. Nieuwe planning windenergie op zee: 21 gigawatt in 2032. (2024). URL: https://www.rvo.nl/nieuws/nieuwe-planning-windenergie-op-zee.

[35] Rijksdienst voor Ondernemend Nederland. Windparken op de Noordzee. (2024). URL: https://www.rvo.nl/onderwerpen/windenergie-op-zee/windparken-noordzee.

[36] Peder C Pedersen, Oleh Tretiak, and Ping He. “Impedance-matching properties of an inhomogeneous matching layer with continuously changing acoustic impedance”. In: *The Journal of the Acoustical Society of America* 72.2 (1982), pp. 327–336.

[37] Yaxi Peng et al. “Modelling and development of a resonator-based noise mitigation system for offshore pile driving”. In: *Proceedings of the 25th International Congress on Sound and Vibration*. 2018.

[38] Haran Periyathamby. “Helmholtz resonator for reducing tire cavity resonance and in-vehicle noise”. In: *Canadian Acoustics* 32.4 (2004), pp. 27–31.

[39] Lord Rayleigh. “The theory of the Helmholtz resonator”. In: *Proceedings of the Royal Society of London. Series A, Containing Papers of a Mathematical and Physical Character* 92.638 (1916), pp. 265–275.

[40] Per G Reinhall and Peter H Dahl. "Underwater Mach wave radiation from impact pile driving: Theory and observation". In: *The Journal of the Acoustical Society of America* 130.3 (2011), pp. 1209–1216.

[41] Ayrton Alfonso Medina Rodríguez et al. "Improved hydrodynamic performance of an OWC device based on a Helmholtz resonator". In: *Energy* 273 (2023), p. 127299.

[42] A Selamet et al. "Theoretical, computational and experimental investigation of Helmholtz resonators: one-dimensional versus multi-dimensional approach". In: *SAE transactions* (1994), pp. 970–979.

[43] Soroush Sepehri et al. "Tunable elastic wave propagation in planar functionally graded metamaterials". In: *Acta Mechanica* 231.8 (2020), pp. 3363–3385.

[44] Karl Friedrich Julius Sondhauss. *Ueber den Brummkreisel und das Schwingungsgesetz der kubischen Pfeifen*. 1850.

[45] Brandon L Southall et al. "Marine mammal noise-exposure criteria: initial scientific recommendations". In: *Bioacoustics* 17.1-3 (2008), pp. 273–275.

[46] John William Strutt and John William Strutt Rayleigh. *The theory of sound*. Vol. 1. Macmillan, 1877.

[47] Nobumasa Sugimoto and T Horioka. "Dispersion characteristics of sound waves in a tunnel with an array of Helmholtz resonators". In: *The Journal of the Acoustical Society of America* 97.3 (1995), pp. 1446–1459.

[48] A Tsouvalas and AV Metrikine. "A three-dimensional vibroacoustic model for the prediction of underwater noise from offshore pile driving". In: *Journal of Sound and Vibration* 333 (8 Apr. 2014), pp. 2283–2311. ISSN: 0022460X. DOI: 10.1016/j.jsv.2013.11.045.

[49] A Tsouvalas and AV Metrikine. "Noise reduction by the application of an air-bubble curtain in offshore pile driving". In: *Journal of Sound and Vibration* 371 (2016), pp. 150–170.

[50] Apostolos Tsouvalas. "Underwater noise emission due to offshore pile installation: A review". In: *Energies* 13.12 (2020), p. 3037.

[51] Apostolos Tsouvalas. "Underwater noise generated by offshore pile driving". PhD thesis. Delft University of Technology Delft, The Netherlands, 2015.

[52] Apostolos Tsouvalas and Andrei V Metrikine. "Parametric study of noise reduction by an air-bubble curtain in offshore pile driving". In: *Proceedings of the ICSV* (2016).

[53] Jianguo Wang et al. "A model to predict acoustic resonant frequencies of distributed Helmholtz resonators on gas turbine engines". In: *Applied Sciences* 9.7 (2019), p. 1419.

[54] X Wang and Cheuk Ming Mak. "Acoustic performance of a duct loaded with identical resonators". In: *The Journal of the Acoustical Society of America* 131.4 (2012), EL316–EL322.

[55] M Wochner et al. "Underwater noise mitigation from pile driving using a tuneable resonator system". In: *Proceedings of the 22nd International Congress on Acoustics, Buanos Aires* (2016).

[56] Mark S Wochner et al. "Attenuation of low frequency underwater noise using arrays of air-flled resonators". In: *INTER-NOISE and NOISE-CON Congress and Conference Proceedings*. Vol. 249. 3. Institute of Noise Control Engineering. 2014, pp. 4048–4054.

[57] MB Xu, Ahmet Selamet, and Hyunsu Kim. "Dual helmholtz resonator". In: *Applied Acoustics* 71.9 (2010), pp. 822–829.

[58] Takashi Yasuda et al. "Studies on an automobile muffler with the acoustic characteristic of low-pass filter and Helmholtz resonator". In: *Applied Acoustics* 74.1 (2013), pp. 49–57.

[59] Yoon Young. *Elastic Waves and Metamaterials: The Fundamentals*. Springer Verlag, Singapore, 2023.

[60] Xuanlie Zhao et al. "Long wave absorption by a dual purpose Helmholtz resonance OWC breakwater". In: *Coastal Engineering* 178 (2022), p. 104203.

A

Appendix: Green's Function

To explain the theory behind the Green's function, the following linear system is considered

$$Lu(x) = f, \tag{A.1}$$

where L is a linear differential operator on the domain $x \in [0, l]$ with prescribed boundary conditions. The solution of this system is easily formulated as

$$u(x) = L^{-1} f. \tag{A.2}$$

Next, consider the Dirac delta function $\delta(x - x_0)$. A specific property of the Dirac delta function is defined as follows

$$\big\langle f(x), \delta(x - x_0) \big\rangle = f(x_0). \tag{A.3}$$

Equation A.3 shows the so called sifting property of the Dirac delta function. The inner product of a forcing function $f(x)$ and the Dirac delta function results in the value of the forcing function at x_0. This is an important property for the construction of a Green's function. In order to solve the Green's function, consider the following steps

$$\big\langle Lu(x), G \big\rangle = \big\langle f, G \big\rangle$$

$$\big\langle u(x), L^* G \big\rangle = \big\langle f, G \big\rangle$$

$$\big\langle u(x), \delta(x - x_0) \big\rangle = \big\langle f, G \big\rangle$$

$$u(x_0) = \big\langle f, G \big\rangle = \int_0^l f(x_0) G(x, x_0) dx_0.$$

B

Appendix: Normal Mode Method

In acoustics, the wave number is the spatial frequency of an acoustic wave (radians per meter). The wave number relates the angular frequency of a wave through a medium to the speed of sound through a medium. In a two-dimensional domain with cylindrical coordinates two wave numbers exist to account for the spatial frequency of the wave in horizontal and vertical direction, these wave numbers are called the horizontal wave number and the vertical wave number, respectively. The form of the horizontal and vertical wave numbers define the type of Hankel function $H_0^{(n)}$ is required. The Hankel functions, or the Bessel functions of the third kind, are linear combinations of the first and second Bessel functions. The Hankel functions express outward- and inward-propagating cylindrical wave solutions of the cylindrical wave equation for $r \to \infty$, and play an important role in correctly implementing geometrical spreading in a cylindrical coordinate system.

$$H_0^{(1)}(kr) = J_0(kr) + iY_0(kr) \simeq \sqrt{\frac{2}{\pi kr}} e^{i\left(kr - \frac{\pi}{4}\right)} \tag{B.1}$$

$$H_0^{(2)}(kr) = J_0(kr) + iY_0(kr) \simeq \sqrt{\frac{2}{\pi kr}} e^{-i\left(kr - \frac{\pi}{4}\right)} \tag{B.2}$$

In [23] the horizontal and vertical wave numbers in a cylindrical coordinate system are derived by applying the normal mode method to the well defined *Isovelocity Problem*, which solves a profile with constant density (and subsequently constant sound speed) over depth. Consider the general solution

$$\Psi_m(z) = A \sin(k_z z) + B \cos(k_z z), \tag{B.3}$$

with vertical wavenumber k_z

$$k_z = \sqrt{\left(\frac{\omega}{c}\right)^2 - k_r^2}. \tag{B.4}$$

Where k_r is the horizontal wavenumber, ω is the angular frequency and c is the speed of sound. At the surface ($z = 0$), a pressure release boundary condition is considered, resulting in $B = 0$. At the seabed ($z = D$), a rigid boundary condition is considered, which leads to

$$Ak_z \cos(k_z D) = 0. \tag{B.5}$$

In this case, either $A = 0$ or

$$k_z D = \left(m - \frac{1}{2}\right)\pi, \quad m = 1, 2, \ldots \tag{B.6}$$

Where m is the mode number. Combining Equation B.4 and Equation B.6 results in the formulation of the horizontal wavenumber

$$k_r = \sqrt{\left(\frac{\omega}{c}\right)^2 - \left[\left(m - \frac{1}{2}\right)\frac{\pi}{D}\right]^2}. \tag{B.7}$$

Equation B.6 and Equation B.7 denote the relation between the frequency and wave number of a complex wave and subsequently the dispersion relation. The real and imaginary parts of the horizontal and vertical wavenumbers are plotted in Figure B.1 for a frequency range between 0 and 300 Hz, i.e. the dispersion relation. It is observed that the real and imaginary part of the wave numbers are positive. Therefore, the Hankel function of the first kind is used for propagating waves in the Green's function (Equation 3.17).

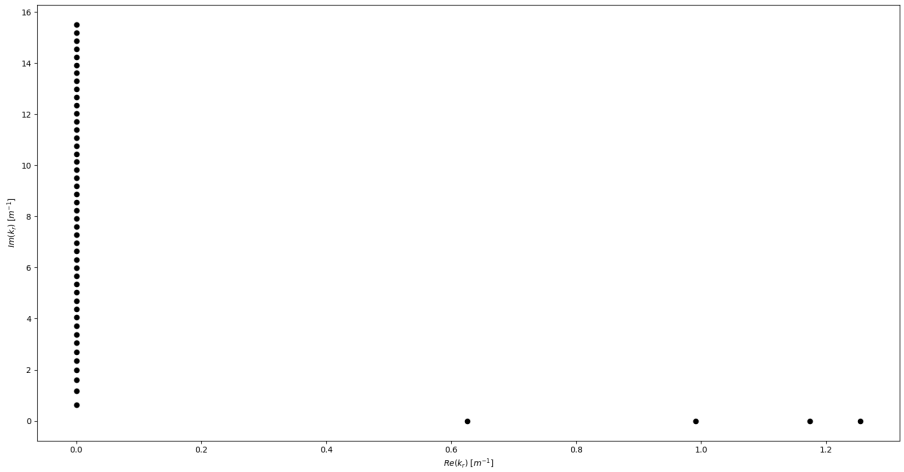

Figure B.1: Dispersion relation for a waveguide with a water depth of $D = 10$ m, 300 Hz.

In the figure below, the horizontal dispersion relation for a waveguide with a water depth of $D = 10$ m is depicted for frequencies from 0 to 300 Hz (e.g. the relation between the horizontal wave number k_r and the frequency). It is observed that for this combination of water depth and frequency range, four propagating modes exist.

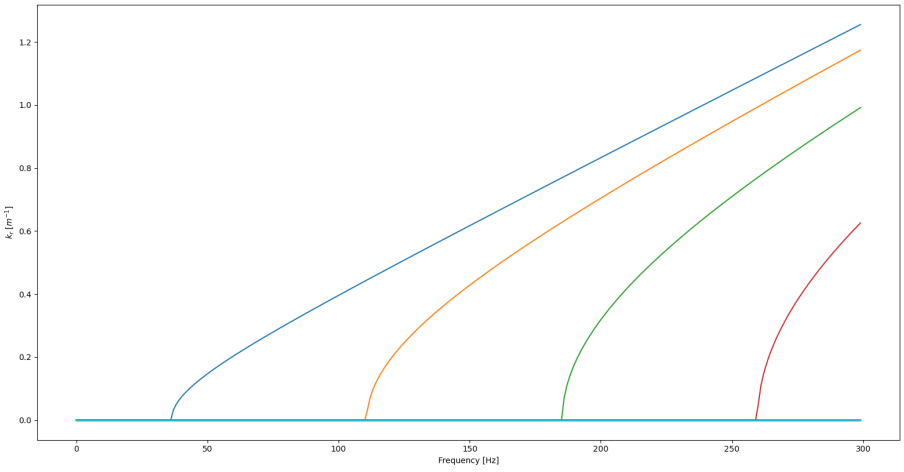

Figure B.2: Dispersion relation for a waveguide with a water depth of $D = 10$ m, 0 to 300 Hz.

In the figure below, the absolute pressure at $r = 4$ m from a monopole point source with unit strength resulting from Equation 3.18 is depicted. Similarly to Figure B.2, the four propagating

modes are clearly visible.

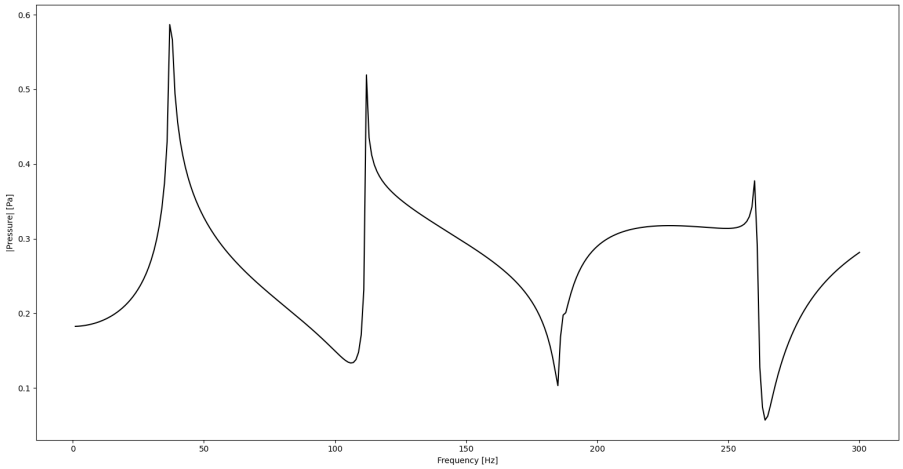

Figure B.3: Absolute pressure in a domain with a water depth of $D = 10$ m exited by a monopole point source with unit strength, measured at 4 m from the source.

C

Appendix: Linear System

Based on a paper by Peng et al. (2018), the method to derive the pressure at the open end of a Helmholtz-type resonator is provided [37]. First, consider the boundary integral formulation for a point source in a bounded medium [23].

$$\tilde{p}(\mathbf{r},\omega) = \int_S \left[G_\omega(\mathbf{r},\mathbf{r}_0)\frac{\partial \tilde{p}(\mathbf{r}_0)}{\partial \mathbf{n}_0} - \tilde{p}(\mathbf{r}_0)\frac{\partial G_\omega(\mathbf{r},\mathbf{r}_0)}{\partial \mathbf{n}_0}\right] dS_0 - \int_V f(\mathbf{r}_0)\, G_\omega(\mathbf{r},\mathbf{r}_0)\, dV_0. \tag{C.1}$$

Substitute the location of the the field location $\mathbf{r}$ by the location of the centre point of the resonator $\mathbf{r}_R$ as $\mathbf{r} = \mathbf{r}_m^R$. The boundary integral formulation then becomes

$$\tilde{p}(\mathbf{r}_m^R,\omega) = \sum_{n=1}^{M}\left\{ \int_{S_n^R}\left[G_\omega\left(\mathbf{r}_m^R,\mathbf{r}_n\right)\frac{\partial \tilde{p}\left(\mathbf{r}_n^R\right)}{\partial \mathbf{n}_0} - \tilde{p}\left(\mathbf{r}_n^R\right)\frac{\partial G_\omega\left(\mathbf{r}_m^R,\mathbf{r}_n\right)}{\partial \mathbf{n}_0}\right] dS_0\right\} - \int_V f(\mathbf{r}_S)\, G_\omega\left(\mathbf{r}_m^R,\mathbf{r}_S\right) dV_0. \tag{C.2}$$

In this formulation, r_m^R is the location of resonator m and the surface of the open end of resonator n is denoted by S_n^R. The spatial derivative is substituted by the frequency response function

$$\frac{\partial \tilde{p}\left(\mathbf{r}_n^R\right)}{\partial \mathbf{n}_0} = \rho_w \omega^2 H(\omega)\tilde{p}\left(\mathbf{r}_n^R\right). \tag{C.3}$$

and every term including the pressure at the open end of the resonator is moved to the left-hand side of the equation. From this, Equation C.2 is represented as a linear system

$$\begin{bmatrix} \mathcal{L}_{1,1}^R & \mathcal{L}_{1,2}^R & \cdots & \mathcal{L}_{1,M}^R \\ \mathcal{L}_{2,1}^R & \mathcal{L}_{2,2}^R & \cdots & \mathcal{L}_{2,M}^R \\ \vdots & \ddots & \vdots & \vdots \\ \mathcal{L}_{M,1}^R & \mathcal{L}_{M,2}^R & \cdots & \mathcal{L}_{M,M}^R \end{bmatrix} \cdot \begin{bmatrix} \tilde{p}\left(\mathbf{r}_1^R,\omega\right) \\ \tilde{p}\left(\mathbf{r}_2^R,\omega\right) \\ \vdots \\ \tilde{p}\left(\mathbf{r}_M^R,\omega\right) \end{bmatrix} = \begin{bmatrix} \mathbf{q}\left(\mathbf{r}_1^R,\omega\right) \\ \mathbf{q}\left(\mathbf{r}_2^R,\omega\right) \\ \vdots \\ \mathbf{q}\left(\mathbf{r}_M^R,\omega\right) \end{bmatrix} \tag{C.4}$$

Where $\mathbf{L}^R = \mathbf{I} + \mathbf{B}^R$

$$\mathbf{I} = \begin{bmatrix} 1 & 0 & \cdots & 0 \\ 0 & 1 & \cdots & 0 \\ \vdots & \vdots & \ddots & 0 \\ 0 & 0 & \cdots & 1 \end{bmatrix}, \quad \mathbf{B}^R = \begin{bmatrix} \mathcal{B}_{1,1}^R & \mathcal{B}_{1,2}^R & \cdots & \mathcal{B}_{1,M}^R \\ \mathcal{B}_{2,1}^R & \mathcal{B}_{2,2}^R & \cdots & \mathcal{B}_{2,M}^R \\ \vdots & \ddots & \vdots & \vdots \\ \mathcal{B}_{M,1}^R & \mathcal{B}_{M,2}^R & \cdots & \mathcal{B}_{M,M}^R \end{bmatrix}. \tag{C.5}$$

The terms $\mathcal{B}_{m,n}^R$ and $\mathbf{q}_m^R$ are defined as follows

$$\mathcal{B}_{m,n}^R = -\alpha S_n^R G_\omega\left(\mathbf{r}_m^R,\mathbf{r}_n^R\right)\rho\omega^2 H(\omega) + \frac{\partial G_\omega\left(\mathbf{r}_m^R,\mathbf{r}_n^R\right)}{\partial z} \tag{C.6}$$

$$\mathbf{q}_m^R = S_\omega G_\omega \left(\mathbf{r}_m^R, \mathbf{r}_S \right) \tag{C.7}$$

By solving this linear system for $\mathbf{p}$, the pressure at the open end of each resonator in the domain is obtained.

D

Appendix: Sensitivity Receiver Location for 1D Periodicity Study

To define the minimal distance of the receiver R from the source S at which the pressure ratio (i.e. mitigated pressure at a specific range r divided by the unmitigated pressure at that same point) remains constant, a sensitivity study is conducted. In Figure D.1, the pressure ratio due to a single resonator at $r = 2$ m from the source is measured at six distances r from the resonator. It is observed that from $r = 2$ m to $r = 16$ m the pressure ratio decreases notably, whereas from $r = 32$ m the pressure ratio converge to constant values. Therefore, in the study of section 5.1 the receiver R is located at a distance of $r = 32$ m from the final resonator in the array.

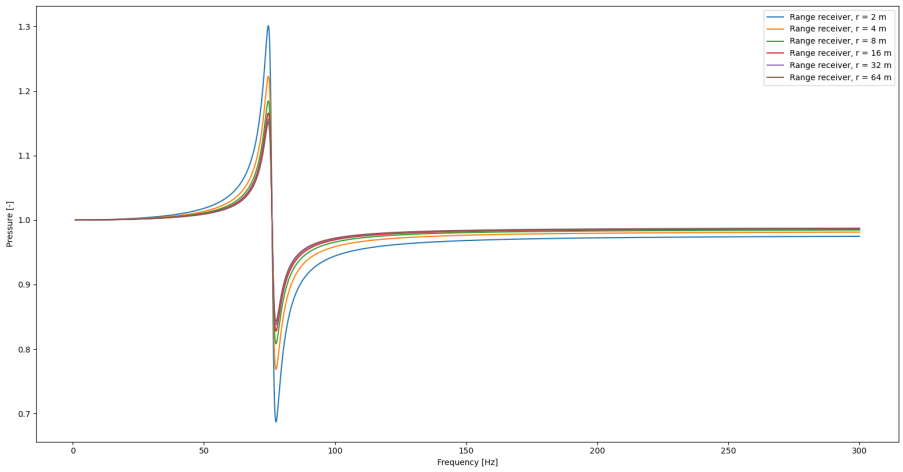

Figure D.1: Caption

E

Appendix: Time Domain Source

The time-domain pressure response of the source is transformed to a frequency-domain response S_ω by use of the Forward Fast Fourier Transform. The frequency-domain response S_ω is then used at input in the boundary integral formulation in the BEM. The pressure response resulting from the BEM calculations are subsequently transformed back to a time-domain response by use of the Inverse Fast Fourier Transform. The Fourier transform pair is included in the equations below.

$$f(t) = \frac{1}{2\pi} \int_{-\infty}^{\infty} f(\omega) e^{i\omega t} d\omega \tag{E.1}$$

$$f(\omega) = \int_{-\infty}^{\infty} f(t) e^{-i\omega t} dt \tag{E.2}$$

In order to successfully apply the Fourier transform pair, the frequency- and time steps have to be carefully defined. Jensen at al. (2011) provide a clear overview of the discretisation of the time and frequency axes for Fast Fourier Transforms. Table E.1 shows the relevant parameters to successfully apply both Fourier transforms in this study.

N_f [-]	4800
N_t [-]	$2 \cdot N_f$
t_0 [s]	0
Δt [s]	$\frac{1}{N_t}$
T [s]	$2 \cdot \Delta t \cdot N_f$
Δf [Hz]	$\frac{1}{T}$
f_0 [Hz]	Δf
f_{max} [Hz]	$0.5\frac{1}{\Delta t}$

Table E.1: Time-stepping.

F

Appendix: Phase Plots

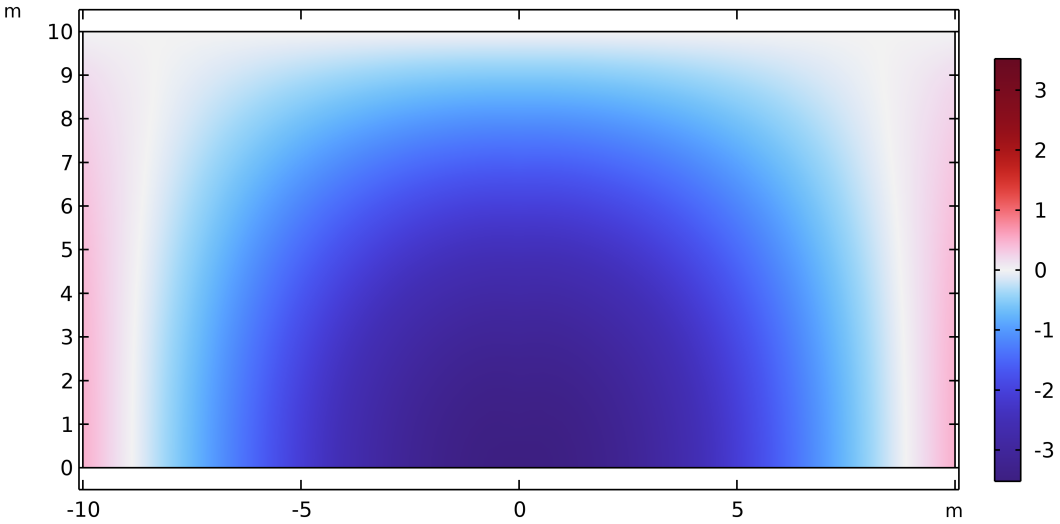

Figure F.1: Phase at 75 Hz

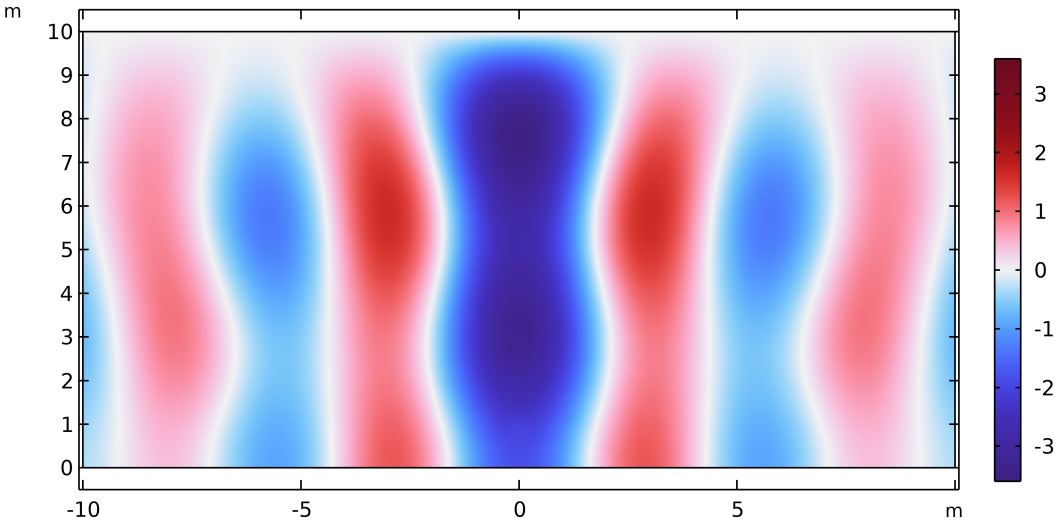

Figure F.2: Phase at 300 Hz